Organelle calcium-derived voltage oscillations in pacemaker neurons drive food-seeking behavior in *Aplysia*

Alexis Bédécarrats, Laura Puygrenier, John Castro O'Byrne, Quentin Lade, John Simmers, Romuald Nargeot

Univ. Bordeaux, INCIA, UMR 5287, F-33076 Bordeaux, France.
CNRS, INCIA, UMR 5287, F-33076 Bordeaux, France.

For correspondence:
Dr Romuald Nargeot,
Institut de Neurosciences Cognitives et Intégratives d'Aquitaine (INCIA)
Université de Bordeaux, CNRS - UMR 5287
Zone nord - bâtiment 2AB - 2ème étage
BP 22
146 rue Léo Saignat
33076 BORDEAUX Cedex
E-mail: romuald.nargeot@u-bordeaux.fr

Abstract

The expression of motivated behaviors depends on both external and internally-arising neural stimuli, yet the intrinsic releasing mechanisms for such variably occurring behaviors remain elusive. In isolated nervous system preparations of *Aplysia*, we have found that irregularly expressed cycles of motor output underlying food-seeking behavior arise from regular membrane potential oscillations of varying magnitude in an identified pair of interneurons (B63) in the bilateral buccal ganglia. This rhythmic signal, which is endogenous and specific to the B63 cells, is generated by organelle-derived intracellular calcium fluxes that activate voltage-independent plasma membrane channels. The resulting voltage oscillation spreads throughout a subset of gap junction-coupled buccal network neurons and by triggering plateau potential-mediated bursts in B63, can initiate motor output driving food-seeking action. Thus, an atypical neuronal pacemaker mechanism, based on rhythmic intracellular calcium store release and intercellular propagation, can act as an autonomous intrinsic releaser for the occurrence of a motivated behavior.

Introduction

Motivated behaviors, such as feeding or sexual activity, are triggered by an interplay between impulsive signals originating within the central nervous system (CNS), peripheral stimuli such as sensory cues, and the positive or negative consequences of an act (Balleine, 2019; Berridge, 2019, 2004; Dickinson and Balleine, 1994; Fujimoto et al., 2019). This combination of flexible extrinsic and intrinsic neural releasers determines both the likelihood of occurrence and the selection of action patterns, which in turn imparts irregularity to the expressed goal-directed behavior. However, depending on sensory experience motivated behaviors can be transformed from variable to regular, rhythmically repeating action patterns that lead to the expression of habits, routines, or compulsive behaviors. The production of such stereotyped repetitive behavior, often reinforced by associative learning processes, is considered to become more strongly dependent upon an automatic internally-arising drive and less sensitive to the sensory consequences of the executed action (Balleine, 2019; Balleine and Dezfouli, 2019; Everitt and Robbins, 2016, 2005). Although the contribution of internal drives to the induction of motivated behavior is recognized, unanswered questions remain about their neural origin and whether the highly flexible expression of a motivated behavior relies on similar inherent neuronal processes as found for rhythmic behaviors generally (Grillner and El Manira, 2020; Marder et al., 2015; Selverston, 2010; Steuer and Guertin, 2019).

A suitable animal model for addressing such issues is the sea slug *Aplysia*, in which aspects of feeding behavior are generated by a well characterized neuronal network within the buccal ganglia. In the absence of food stimuli, *Aplysia* spontaneously expresses food-seeking behavior, which in addition to locomotor and head-waving movements, includes buccal and

radula (a tongue-like organ) biting movements emitted at highly irregular intervals (Kupfermann, 1974). This spontaneous and variable behavior can be regulated by operant-reward conditioning that leads to the expression of regular and rhythmic biting movements (Brembs et al., 2002; Costa et al., 2020; Nargeot et al., 2007; Sieling et al., 2014). Importantly, neural correlates of this motivated behavior continue to be expressed by the underlying neuronal network in the isolated buccal ganglia, thereby enabling the mechanisms responsible for autonomously driving both the irregular and regular emissions of radula movement cycles to be analyzed at the cellular and synaptic levels (McManus et al., 2019; Nargeot and Simmers, 2012). Identified components of this central pattern generator (CPG) circuit, such as the electrically-coupled B63, B30, B31/32 neurons, were previously found to be essential contributors to the decision-making process that drives radula motor output (Costa et al., 2020; Hurwitz et al., 1997; Jing et al., 2004; Nargeot et al., 2009; Sieling et al., 2014; Susswein and Byrne, 1988). Among these elements, the two bilateral B63 interneurons are the only cells whose spontaneous production of an action potential burst is necessary and sufficient to trigger each radula output cycle (Nargeot et al., 2009). Thus, deciphering the mechanisms underlying the endogenous bursting activity of these key decision neurons is critical to understanding the process of radula motor pattern expression. Although B63 bursting and buccal network activity were previously found to rely on the cell's plateau potential-generating capability and its electrical synapses with other circuit neurons (Sieling et al., 2014; Susswein et al., 2002), the mechanism responsible for spontaneously triggering B63 plateaus and consequently the irregular emission of motor output remains unknown. Our findings reported here indicate that such motor pattern genesis relies on a voltage-insensitive pacemaker mechanism originating

from organelle-driven fluxes in intracellular calcium that is specific to this homologous pair of neurons.

Results

Motor output responsible for radula biting behavior, which in the absence of any food stimulation consists of irregularly recurring cycles of radula protraction, closure and retraction (Figure 1A), continues to be expressed by identified CPG circuitry in isolated buccal ganglia (Figure 1B) and can be recorded from the corresponding buccal motor nerves (Figure 1C). Individual radula bites are instigated by synchronous impulse burst activity in the two bilateral, electrically-coupled B63 interneurons that via electrical and chemical synapses with their ipsi- and contralateral buccal network partners, are able to trigger the two-phase buccal motor pattern (BMP) for a bite cycle (Figure 1C) (Hurwitz et al., 1997; Nargeot et al., 2007; 2009). This essential role played by B63 is partly mediated by a bistable membrane property, which allows the sudden switching of the neuron's resting membrane potential to a depolarized plateau that activates a high frequency burst of action potentials (Susswein et al., 2002). Consistent with this property's regenerative nature, a brief intracellular injection of depolarizing current into an otherwise silent B63 neuron can initiate a plateau potential and accompanying burst discharge, which in turn activates the contralateral B63 cell and elicits a single BMP by the buccal CPG network (Figure 1D).

A rhythmic oscillatory drive underlies irregular BMP genesis

To investigate the mechanism(s) responsible for spontaneously instigating B63's plateau potentials and resulting BMPs, we first sought evidence for an underlying triggering process in stable intracellular recordings from this neuron in still active isolated buccal ganglia (N = 26) in the absence of any electrical or chemical stimulation. Such recordings (episodes of >10 min per cell) revealed that B63's membrane potential underwent continuous depolarizing fluctuations over time (Figures 1C, 2A), many of which remained below threshold for action and plateau potential generation. Others of these low-amplitude depolarizations elicited isolated action potentials without a plateau potential, whereas the remainder were associated with the production of a plateau potential and the expression of a BMP. Consequently, B63's plateau potentials and fictive bite cycles were spontaneously generated at irregular time intervals ranging from several seconds to a minute.

Although B63's widely variable plateauing activity was expressed in an apparently random manner, we next asked whether its recurrence was associated with a specific temporal organization in the cell's membrane potential fluctuations. To assess this possibility, Fourier (spectral) analysis (see Material and Methods) was applied to 10 min excerpts of the 26 B63 cell recordings. As seen in the spectral density periodogram for the B63 neuron illustrated in Figure 2A, the cell's spontaneous membrane potential changes decomposed into two distinct periodicities with peaks at 61 s and 144 s, respectively (Figure 2B, upper panel; Supplemental Figure 1). Moreover, a mathematical reconstruction based on these dominant periods showed that the slower waveform was mostly correlated with the largest membrane potential depolarizations that led to plateau potentials and the production of BMPs (Figure 2C). In contrast, the faster waveform was timed with virtually all membrane voltage changes, including

the subthreshold fluctuations and events associated with isolated action potentials or plateau potential-driven bursts.

The faster of the two periodicities (mean ± CI95, 58 ± 5 s) varied relatively little between different preparations, as evidenced by the sharper spectral density peak in the averaged periodogram for all 26 buccal preparations (Figure 2B, lower panel). In contrast, the broader peak of the slower rhythm (mean ± CI95, 146 ± 23 s) was indicative of the wide variability in occurrence of plateau potentials over time and between preparations. Moreover, for both rhythms, the considerable variability in their power spectral magnitudes (1592 ± 650 mV^2.s, 1524 ± 676 mV^2.s; mean ± CI95%, respectively) was attributable to the large amplitude variations between spontaneous membrane depolarizations that succeeded or failed to trigger plateau potentials in the different preparations (see also, Supplemental Figure 1A ,B).

To further characterize the temporal nature of B63's faster oscillatory rhythm, spectral analysis was performed on cells (N = 14) that did not produce plateau potentials and resultant BMPs throughout 10 min recording sequences. Such non-plateauing neurons continued to express repetitive, now uniquely sub-threshold, membrane depolarizations (Figure 2D) that again were clearly rhythmic as revealed by the single dominant peak both in individual (Figure 2E, top). and averaged periodograms of the 14 recorded neurons (Figure 2E, bottom). Moreover, the mean period (± CI95%) of this solitary rhythm (69 ± 7 s) was within a range equivalent to that of the faster oscillatory waveform found in B63 neurons that additionally expressed plateaus (cf, Figure 2E, B). Although the magnitude of the remaining subthreshold rhythm varied over time and between preparations (Figure 2E, Supplemental Figure 1B), as also

evidenced by waveform reconstruction (Figure 2F), it had a much smaller amplitude than the corresponding waveform in plateau-active cells.

Altogether, these results show that the B63's spontaneous bioelectrical behavior includes a rhythmic depolarizing signal that can remains below threshold for neuronal excitability or, in an apparently random manner, can lead to action and plateau potential production. However, despite their irregularity, the expression of plateau potentials, and resultant BMPs, is also inscribed with a periodicity, albeit considerably slower and more variable than the underlying oscillation.

The voltage oscillation is endogenous to B63 and drives plateauing

In principle, the low amplitude oscillation of the B63 neurons could originate extrinsically from a presynaptic source, or derive intrinsically from a rhythmogenic property inherent to the neurons itself. Although no other buccal ganglia cell has been found to provide such a synaptic drive, we distinguished between these two possibilities by recording B63 cells in isolated preparations in which chemical synapses were blocked by bath perfusion of a modified saline containing a low calcium concentration (3 mM) and 10 mM cobalt, a nonspecific calcium channel blocker.

The application of such 'Low Ca+Co' saline soon induced a prolonged depolarization of recorded B63 neurons (Figure 3A), then after ca. 20 min, which was necessary to fully block chemical synapses - as confirmed by the suppression of the excitatory synapse between B63 and a contralateral B31 neuron (data not shown) - the membrane potential repolarized to its initial level. Significantly, these neurons thereafter continued spontaneously to express a low-

amplitude oscillation for > 1.5 hrs, although its magnitude gradually decreased over time (see Supplemental Figure 6A). As in normal saline conditions, the cyclic depolarizations were either sub- or supra-threshold for spike generation, or at irregular intervals, were associated with plateau potentials and high frequency bursts (Figure 3A, B; Supplemental Figure 2).

Spectral analysis of these persistent membrane potential oscillations during 20 min recording periods after chemical synapse blockade in 15 buccal ganglia preparations revealed that, as in ASW conditions, B63's membrane potential fluctuations decomposed into two major periodicities (Figure 3B, C and Supplemental Figure 1C). The periodograms and corresponding waveform reconstructions indicated that the slowest oscillation (mean period ± CI95%: 274 ± 61 s) of large magnitude (mean spectral density ± CI95%: 11587 ± 5741 $mV^2.s$) was mainly associated with the expression of plateau potentials. The fastest oscillation (mean period ± CI95%: 104 ± 12 s) of smaller amplitude (mean spectral density ± CI95%: 4640 ± 3341 $mV^2.s$) corresponded to rhythmic depolarizations that remained subthreshold, or were associated either with low frequency spiking or plateau driven bursts. As found in unblocked ganglia, this faster periodicity was more clearly evident when plateauing was absent: in 10 of the 15 buccal ganglia, B63 failed to produce plateaus during at least 10 min of analyzed recording excerpts, although these neurons continued to spontaneously express a rhythmic subthreshold oscillation (Figure 3D, E and Supplemental Figure 1D). Again, the mean cycle period of this solitary waveform (± CI95%: 98 ± 8 s) was similar to that of the faster rhythm when plateau potentials also occurred (cf., Figure 3B, C).

Thus, although blocking chemical synapses led to variations in mean cycle periods, amplitudes and plateau durations, B63's spontaneous voltage fluctuations still expressed two

196 distinct oscillatory states, indicating that both processes occur independently of chemical
197 synaptic inputs. Furthermore, inspection of the superimposed reconstructions of these
198 oscillations under Low Ca+Co (Figure 3B), as in ASW (see Figure 2C), indicated that the onset of
199 each plateau potential was invariably associated with a depolarizing phase of the faster
200 oscillation, suggesting that the latter endogenous signal might be responsible for triggering the
201 former.

202 This initiating process was further indicated by comparing the kinetics of B63's
203 spontaneous voltage changes during subthreshold cycles of oscillation with those associated
204 with plateaus. From recordings under both synaptic blockade (Figure 4A,B) or normal saline
205 conditions (Supplemental Figure 3A), the superposition of single cycles with and without
206 plateau potential occurrences indicated that the relatively fast rising phases of the two events
207 shared similar trajectories. In the absence of a plateau potential, this initial depolarization could
208 trigger large amplitude impulse firing, or when a plateau occurred, it emerged as an additional
209 and sustained (lasting tens of seconds) depolarization of 20-30 mV that in turn elicited a high
210 frequency burst of low amplitude action potentials. The relationship between the voltage
211 oscillation and plateauing in both Low Ca+Co and ASW conditions was quantified by phase
212 plane analysis, which enables visualizing the voltage trajectory of neuronal oscillatory activity
213 independent of time. To this end, recordings from B63 were low pass filtered to remove action
214 potentials, then membrane voltage was plotted against the first derivative dV/dt, which is
215 proportional to the net membrane ionic current (Zhu et al., 2016). Such phase-plane plots from
216 data excerpts of the same neurons under synaptic blockade (Figure 4C) or unblocked conditions
217 (Supplemental Figure 3B) clearly showed a close coincidence between the early depolarizing

trajectories of the spontaneous oscillation whether they developed (black spirals) or not (red spirals) into a sustained plateau. Subsequently, depending on the membrane potential reached at the end of this initial phase, the level of which varied considerably from one cycle to another, the trajectories bifurcated to give rise either to the large and stereotyped voltage changes of plateau potentials, or if subthreshold, immediately spiraled back to the baseline potential.

Therefore, together these results support the conclusion that rather than being instigated by chemically-mediated synaptic inputs, the repeated expression of plateau potentials by the B63 neuron is a direct consequence of a spontaneous membrane voltage oscillation of irregular magnitude originating from within the cell itself.

The oscillatory mechanism is not voltage-dependent

A classical diagnostic feature of endogenous neuronal oscillators, the inherent rhythmogenic capability of which typically derives from voltage- and time-dependent membrane channels, is a sensitivity of cycle frequency and mode of firing to different levels of membrane polarization (Bal et al., 1988; Canavier et al., 1991; Mathieu and Roberge, 1971). We therefore tested the voltage-dependence of B63's oscillatory mechanism by manipulating the cell's membrane potential during intracellular recordings from buccal ganglia exposed to Low Ca+Co saline. As described earlier in this condition, B63 neurons continued spontaneously to generate a voltage oscillation that included both subthreshold depolarizations and less frequent plateau potentials with accompanying intense bursts of impulses (Figure 5A, left). As seen in Figure 5A (right), a continuous experimental hyperpolarization by intracellular current injection suppressed the expression of plateau potentials, but with no observable effect on the frequency of the

underlying oscillation. The latter remained similar to that expressed before the imposed hyperpolarization where individual depolarizing cycles were strictly time-locked with the raising phase of each plateau potential (see arrowheads in Figure 5A, left). These findings were therefore in accordance with the all-or-none, voltage-sensitivity of B63's plateau potentials that are activated by the low-amplitude voltage oscillation. They also indicated that the latter's cycle period is unaffected by a change in membrane potential either in response to experimental manipulation or during the plateau potentials themselves.

This voltage-insensitivity of B63's low amplitude oscillation was further established by comparing the effects of the same imposed membrane potential changes in different preparations. Using two-electrode current-clamp in 7 preparations, B63 was initially held at -70 mV, a potential that was subthreshold for plateau genesis, and subsequently further hyperpolarized to -80 mV. No significant change in oscillation cycle period resulted from this hyperpolarization (Figure 5B, C; V = 16, p = 0.799). Similarly, in 9 preparations continuous depolarizing current injection that shifted B63's membrane potential from -70 mV to -30 mV also had no significant effect on the period of ongoing oscillation (Figure 5D, E; V = 28, p = 0.553). In contrast to the cycle period, however, in the same experiments the amplitude of B63's oscillation was found to increase (Figure 5B) or decrease (Figure 5D) according to the sign of injected current. Presumably this was due to the membrane potential shifting relative to the reversal potential of the depolarizing inward currents producing the oscillation (see below). Finally, very similar observations were made from a different set of B63 neurons also recorded in unstimulated buccal ganglia but which remained under ASW (data not shown), thereby

confirming that the cell's voltage-independent oscillation was a spontaneous emergent property regardless of whether the buccal network remained functionally reduced or intact.

Altogether, these results are consistent with an expected contribution of intrinsic, voltage-dependent channels to plateau potential genesis in the B63 neuron, and confirm that they are triggered by the underlying voltage oscillation. On the other hand, however, our data show that the mechanism responsible for the oscillation itself does not rely on an activation of voltage-dependent ion channels in the neuron's membrane.

Circuit-wide voltage oscillation via gap-junction coupling

Although chemical synaptic interactions with other buccal network neurons are not responsible for generating B63's low-amplitude voltage oscillation, the possibility remained that it originates extrinsically and is conveyed to B63 through electrical synapses, which are widespread in buccal CPG circuitry. To assess this possibility, simultaneous intracellular recordings of B63 with at least one another electrically-coupled neuron of the buccal CPG network (see Figure 1B) were made under Low Ca+Co saline. Because the B63, B31 and B30 neurons in each of the bilateral ganglia are major components of the radula protraction generator subcircuit and share strong electrical synapses (Hurwitz et al., 1997; Nargeot et al., 2007) these three cell types were chosen for paired recordings. Other protraction generator neurons electrically coupled with B63, such as B34, B65, were also occasionally recorded, while B8 radula closure motor neurons, which are connected to these neurons via chemical, but not any electrical, synapses were used as a control (Costa et al., 2020).

Paired recordings from the bilateral B63 neurons, which are themselves electrically coupled, revealed that the two cells express almost identical low-amplitude oscillations that occur in strict synchrony (Figure 6A). However, action and plateau potentials, whose expression presumably depends on individual cell excitability, occurred independently. Moreover, within a same ganglion, B31 and B30 neurons belonging to the protraction generator and electrically coupled with the ipsilateral B63 also expressed a voltage oscillation in time with that of the latter (Figure 6B; Supplemental Figure 4). In contrast, B8 motor neurons, which are not coupled with B63 or the other protraction generator neurons, did not express any such oscillation (Figure 6C).

The amplitudes and phase relationships of the low-amplitude voltage oscillations in neuronal pairs were next quantified by spectral analysis over 5 successive cycles during which no plateauing occurred. The oscillation magnitude was determined from the peak spectral density of the single dominant period in the corresponding power spectrum (see Supplemental Figure 1D). For homologous bilateral neurons, no significant difference in oscillation amplitude was found between either the B63 or B31 cell pairs (Figure 6D, left; B63/B63, $V = 22$, $p = 0.625$; B31/B31, $V = 13$, $p = 0.687$). However, comparison between heterologous neuron pairs within a same ganglion showed that the oscillation magnitude was significantly greater in B63 than in either the ipsilateral B31 or B30 cells (B63/B31, $V = 78$, $p < 0.001$; B63/B30, $V = 36$, $p < 0.01$) and predictably, in B8 motor neurons (Figure 6D, middle and right; also see 6B and Supplemental Figure 4).

Bivariate cross-waveform analysis of the same recordings revealed no significant phase difference in the voltage oscillations of homologous cell pairs, either between the two B63 or

304 B31 neurons, in bilateral ganglia (Figure 7A, C; B63/B63, V_0 = 31, p = 0.769; B31/B31, V_0 = 15, p
305 = 0.437). Unexpectedly, however, in heterologous ipsilateral pairs, B63's oscillation was found
306 to be significantly phase-advanced by several seconds compared to the accompanying
307 oscillation of either the B31 or B30 neurons (Figure 7B, C; B31/B63, V_0 = 78, p < 0.001; B30/B63,
308 V_0 = 35, p < 0.02). Moreover, group pair-wise comparisons indicated that the oscillation phase
309 was also significantly different between the different cell combinations (H = 20.947, p < 0.001),
310 specifically, between homologous and heterologous pairs (B63/B63 vs B31/B63: q = 6.986, p <
311 0.001; B63/B63 vs B30/B63: q = 8.263, p < 0.001; B31/B31 vs B31/B63: q = -5.064, p < 0.01;
312 B31/B31 vs B30/B63: q = -6.407, p < 0.005). In contrast, no significant phase differences were
313 found between either homologous or between heterologous cell pairs (B63/B63 vs B31/B31: q
314 = 0.889, p = 0.922; B31/B63 vs B30/B63: q = 2.034, p = 0.486).

315 These findings thus showed that a spontaneous membrane potential oscillation is not
316 restricted to the B63 neurons, but extends to all other neurons with which these two cells are
317 electrically-coupled in the radula protraction generator circuit. The voltage oscillations in
318 homologous cells in the two hemi-ganglia are synchronous and with similar amplitudes.
319 However, within a given ganglion, each cycle of oscillation is expressed earlier in B63 and with a
320 greater magnitude than in any of the cell's network partners. These relative timing and
321 amplitude differences therefore support the conclusion that the voltage oscillation is not an
322 equivalent emergent property of a network of electrically-coupled neurons, but rather,
323 originates in the two B63 cells and then spreads, presumably via gap junctional connections
324 with adjacent cells, throughout the remaining circuit.
325

Involvement of cation channels and organelle signaling in B63's oscillation

As reported above, an experimental depolarization of B63 decreased the amplitude of its spontaneous voltage oscillation, indicating a reversal potential for the underlying ionic currents above -30 mV (see Figure 5D), which in turn suggested the involvement of sodium and/or calcium conductances in the oscillation. To test this likelihood, we examined three groups of 6 isolated buccal ganglia that were all initially bathed in Low Ca+Co saline to block chemical synapses. In a first group, the sodium channel blocker, TTX (50 µM), was then added to the bathing solution; in a second 'sodium free' group, the ganglia were exposed to a modified Low+Ca saline in which sodium was replaced by choline, a non-permeable cation; in a third 'calcium-free' group, the initial saline was replaced by a solution lacking any calcium and containing the calcium chelator EGTA (0.5 mM).

As evidenced by the individual cell recordings in Figure 8A-C, the voltage oscillation of the B63 neurons was reversibly abolished by exposure to each of the three salines. This suppression was quantified in the 18 recorded neurons by making a paired comparison of their peak spectral densities in 10 min data excerpts obtained before and after 10 min of modified saline application (Figure 8D). In all cases, the initial dominant oscillation was significantly diminished in each of the saline conditions (TTX: $V = 21$, $p < 0.05$; Sodium-free: $V = 21$, $p < 0.05$; Calcium-free: $V = 21$, $p < 0.05$). A noticeable difference, however, was that from the instant when observable saline effects began to occur, the time course of this suppression varied considerably according to the saline condition. Whereas B63's oscillation terminated totally and abruptly in TTX-containing and Na-free salines (Figure 8A, B), with the same rate of calcium-free perfusion, the oscillation persisted after an effect first became evident, damping

slowly until its full suppression several minutes later (Figure 8C). This difference in oscillation longevity is further evident in the group analysis of Figure 8E, which compares the time until the oscillation ceased when measured from the onset of each modified saline's perfusion. Again, suppression took significantly longer in the Ca-free saline as compared to either the TTX-containing or Na-free conditions ($H = 11.684$, $p < 0.001$; Ca-free vs TTX: $q = 4.624$, $p < 0.05$ and Ca-free vs Na-free: $q = 8.092$, $p < 0.001$), which themselves were not significantly different ($q = -3.468$, $p = 0.07$).

These results are therefore consistent with sodium and calcium ions play a critical role in B63's spontaneous voltage oscillation, although their contributions appear to be fundamentally different. The rapid and full suppression of the oscillation in sodium-free or TTX-containing salines, both of which contained calcium, indicated that TTX-sensitive sodium channels are essential to producing the oscillation. By contrast, its slow decline in the absence of extracellular calcium is not consistent with a primary role of transmembrane calcium influxes in oscillation genesis *per se*. Rather, although necessary for oscillation, calcium may act in an underlying regulatory process involving the dynamics of intracellular calcium and its control by intracellular stores, and that this signal is temporarily preserved after the cation's extracellular removal as the store calcium gradually runs down until depletion.

The main organelles that regulate intracellular calcium concentration are the endoplasmic reticulum (ER) whose membrane carries calcium channels, the calcium-ATPase reuptake pump (SERCA) and calcium release channels (the inositol triphosphate (IP3) and ryanodine (Ry) receptors), and mitochondria that act in energy supply as well as calcium sequestration and release (Groten et al., 2013). To test the implication of ER and mitochondrial

calcium in B63's voltage oscillation, isolated buccal ganglia (N = 6) were bathed in Low Ca+Co saline before and after addition of 20 µM CPA, a selective inhibitor of SERCA (see Materials and Methods). In a second group of ganglia, (N = 6), the same protocol was used, but with the addition of 20 µM FCCP, an oxidative phosphorylation uncoupling agent that leads to calcium release from mitochondrial stores. From intracellular recordings of B63 neurons in these preparations, peak spectral density magnitudes during a 10 min excerpt before drug application - and in the absence of plateau potentials - were compared to those computed over a 10 min period that began 20 min after the start of drug perfusion.

Bath perfusion of CPA caused a progressive and complete, but reversible, suppression of B63's voltage oscillation in association with a slight, but consistent, gradual membrane depolarization (Figure 9A). The application of FCCP also completely, although irreversibly, suppressed the oscillation that was now accompanied by a stronger sustained depolarization of ~10-20 mV (Figure 9C). No such change in B63's voltage oscillation or baseline membrane potential resulted from perfusion of either Low Ca+Co alone or this saline containing solely the DMSO vehicle (Supplemental Figure 5). A within group analysis of peak spectral densities before *vs* during drug application confirmed that exposure to CPA or FCCP significantly reduced the oscillation amplitude of all the recorded B63 neurons (Figure 9B, D; CPA: $V = 21$, $p < 0.05$; FCCP: $V = 21$, $p < 0.05$). The peak spectral density reduction was also significantly different between both the CPA and FCCP experimental groups and neurons exposed to DMSO alone, but not between the CPA and FCCP groups themselves ($H = 11.415$, $p < 0.01$; CPA vs DMSO: $q = 7.018$, $p < 0.001$; FCCP vs DMSO: $q = 6.517$, $p < 0.001$; CPA vs FCCP: $q = 0.501$, $p = 0.933$).

These data are therefore consistent with the hypothesis that intracellular organelles play an important role in generating the B63 neuron's low-amplitude voltage oscillation by a dynamic regulation of intracellular calcium concentration via the release of store calcium and its sequestration mediated by ATP-dependent pumps. Depletion of mitochondrial calcium (induced by FCCP) or of ER calcium by an impairment of reuptake pumps (by CPA) would be expected to block this dynamic, leading to a rise in intracellular calcium levels and a resultant tonic cell membrane depolarization, which is precisely what we observed in the experiments reported above (see Figure 9A, C).

To further establish the ER's involvement in B63's voltage oscillation, a final series of experiments were conducted in which we assessed the effects of blocking the membrane calcium channels of the organelles themselves. This was achieved by pressure injecting heparin (20 mg/ml), a well-known non-permeable IP3 receptor antagonist (Bezin et al., 2008), into the somata of either bilateral pairs of B63 neurons, or their two B31 network partners. After 30 min injection, simultaneous intracellular recordings were made from heterologous B63 and B31 cell pairs under Low Ca+Co saline conditions. Heparin injection into the two B31 neurons had no effect on the ongoing voltage oscillation of either a heparin-injected B31 itself or its non-injected B63 partner (Figure 10A). In contrast, the reverse experiment that consisted of injecting the IP3 receptor antagonist into the two B63 neurons caused a drastic reduction in the spontaneous oscillation, both of one of the injected B63 cells and a recorded B31 partner (Figure 10C). These findings were further supported by spectral analysis of recording excerpts from B63 cells in the two groups of preparations after bilateral B31 (N = 4) or B63 (N = 5) heparin injection. Recorded B63 neurons continued to express a distinct voltage oscillation with

413 a mean period of 67 ± 3.2 s when heparin was injected into the two B31 cells (Figure 10B), but
414 this dominant oscillation disappeared with heparin's presence in the B63 neurons (Figure 10D).
415 Therefore, in addition to the participation of ER calcium sequestering pumps, organelle calcium
416 release via IP3-dependent calcium channels evidently contributes to the voltage oscillation of
417 buccal CPG network neurons. Significantly moreover, these results further demonstrated that
418 the voltage oscillation's origin is specific to the B63 neurons, the sole necessary and sufficient
419 elements for triggering the BMPs that drive radula food-seeking movement.
420

Discussion

This study aimed to decipher the basic neuronal mechanisms underlying a central network's ability to generate the impulsive motor drive for an aspect of *Aplysia's* food-seeking behavior. Our findings indicate that this highly irregular motivated act arises from an atypical endogenous pacemaker property of a homologous pair of decision-making interneurons belonging to the animal's buccal feeding network. The cell-specific pacemaker signal does not derive from an oscillatory mechanism based on voltage-dependent ionic currents, as is usually found, but rather depends on a cyclic release/reuptake of calcium from intracellular stores acting on voltage-insensitive membrane channels. The resultant low amplitude oscillation of the decision neurons' membrane potential, which is spontaneously expressed with a regular period but a varying magnitude, is spread to gap junction-coupled network partners. Depending on the membrane potential reached during the depolarizing phase of a given oscillation cycle, a prolonged plateau and accompanying spike burst may be initiated, which in turn elicits network output for a cycle of food-seeking movement. The intracellular calcium oscillation originating in two key circuit neurons thus provides a continuous rhythmic carrier signal from which burst-generating plateau potentials necessary for behavioral action can sporadically arise.

Intracellular calcium oscillation as a neuronal pacemaker mechanism

The endogenous oscillatory capability of invertebrate and vertebrate neuronal pacemakers is mainly attributed to sets of plasma membrane ion channels whose specific functional properties allow the production of cyclic membrane depolarization/repolarization and associated impulse bursting (Adams and Benson, 1985; Brocard et al., 2013; Calabrese, 1995;

443 Chevalier et al., 2016; Golowasch et al., 2017; Harris-Warrick, 2002; Selverston, 2010). Although
444 this pacemaker mechanism can be regulated by second-messenger cascades and cytosolic
445 calcium released from intracellular stores, its expression relies essentially on the voltage-
446 sensitivity of the membrane channels themselves (Butera et al., 1996; Canavier et al., 1991;
447 Kadiri et al., 2011; Liu et al., 1998; Yu et al., 2004). Thus, depending on membrane potential
448 levels, the cycle frequency of the endogenous voltage oscillation can be modified, thereby
449 changing the frequency of the effector rhythm in which the pacemaker cell is involved
450 (Canavier et al., 1991; Chevalier et al., 2016; Koshiya and Smith, 1999; Miller and Selverston,
451 1982). Spontaneous neuronal oscillations can also be generated by voltage-independent
452 pacemaker mechanisms involving plasma membrane ionic pumps, such as Na/K ATPase, which
453 periodically repolarize the membrane of bursting neurons (Darbon et al., 2003; Johnson et al.,
454 1992; Kueh et al., 2016). Such pump-driven oscillations require tonic cellular activation or
455 disinhibition and are not blocked by extracellular calcium removal or Na channel blockers such
456 as TTX.

457 An increasing body of evidence from studies on endocrine, muscle and non-excitable
458 tissues (Baker et al., 2016; Fridlyand et al., 2010; Vinogradova et al., 2005; Zhou et al., 2019),
459 but also in early developing neurons (Gu et al., 1994), has indicated that a slow oscillatory cell
460 signal with cycle periods of seconds to several minutes can be generated spontaneously by
461 organelle-derived fluctuations in intracellular calcium concentration. Such a rhythmic calcium
462 dynamic, involving notably the endoplasmic reticulum and mitochondria, may be a source of
463 plasma membrane voltage oscillation without the participation of voltage-sensitive ion
464 channels. Specifically, the oscillation arises from a periodic accumulation/removal of

cytoplasmic calcium, principally by IP3 and Ry receptor-mediated calcium efflux and ATP-dependent pump-mediated influx across the store membrane, which in turn is translated into a voltage signal by an activation of calcium-sensitive channels at the plasma membrane (Fridlyand et al., 2010; Hickey et al., 2010; van Helden et al., 2000; Vinogradova et al., 2005).

In a corresponding and novel manner for a neuronal system, our present data indicate that an intracellular calcium wave generated by organelle calcium release and reuptake is responsible for the spontaneous low-amplitude voltage oscillation observed in B63 neurons. First, experimental manipulation of the cell's membrane potential over voltage ranges where most voltage-dependent channels would be expected to be closed had no effect on either the occurrence or frequency of this persistent oscillation. Second, at variance with a possible essential contribution of plasma membrane sodium or calcium pumps, the voltage oscillation was suppressed in TTX-containing saline and its magnitude increased, rather than decreased, as would be expected with low extracellular calcium concentrations. Third, the voltage oscillation was suppressed with pharmacological treatments that inhibit IP3 receptors, block SERCA pumps involved in transporting calcium into the endoplasmic reticulum, and disrupt energy production and calcium storage by mitochondria. Finally, the slow and gradual suppression of the voltage oscillation observed during prolonged exposure to calcium-free saline was commensurate with a progressive depletion of store calcium. Presumably, the primary intracellular calcium dynamic drives plasma membrane voltage oscillation by activating calcium-sensitive and voltage-insensitive sodium or other cation channels (Hickey et al., 2010; Kadiri et al., 2011; Kramer and Zucker, 1985), without excluding the possibility that B63's membrane carries other burst-generating oscillatory properties (Costa et al., 2020; Nargeot et al., 2009; Susswein et al., 2002).

Indeed, in contrast to the organelle-derived oscillatory mechanism reported here, where B63 was behaving spontaneously in the absence any experimental stimulation, this cell also possesses an oscillatory bursting capability that does rely on voltage-dependent ion channels (Nargeot et al, 2007; 2009; Sieling et al, 2009). However, this latter mechanism is activated only when the cell is conveyed to more depolarized levels by sensory-induced changes in excitability or in response to direct current injection. This state-dependent expression of two different burst-generating processes by the B63 neuron is therefore reminiscent of the multiple rhythmogenic ionic mechanisms reported in other oscillatory neurons, where each mechanism's participation varies according to different stimulus conditions (Harris-Warrick and Flamm, 1987; Kadiri et al., 2011; Peña et al., 2004).

Variability in motor pattern emission with a periodic pacemaker mechanism

Irregularity in the expression of motor activity is a fundamental feature of motivated or goal-directed exploratory behaviors, including *Aplysia's* food-seeking movements, when animals are faced with an uncertain surrounding environment. Although such motor variability is partly dictated by peripheral sensory inputs (Cullins et al., 2015; Lyttle et al., 2017; McManus et al., 2019; Pearson, 2000; Tam et al., 2020; Wimmer et al., 2015), it also depends on the functional properties of the central networks and constituent neurons producing the behavior (Sims et al., 2019). In this context, random processes such as stochastic variations in the activation of intrinsic and voltage-dependent properties of individual neurons and synaptic noise can be sources of variability in motor output expression (Carroll and Ramirez, 2013; Darshan et al., 2017; Melanson et al., 2017; Nargeot et al., 2009; Zhang et al., 2020). Moreover, modelling

evidence has suggested that an aperiodicity in slow cytosolic calcium dynamics can lead to irregular voltage oscillations in otherwise regularly bursting CPG neurons (Falcke et al., 2000). In contrast, our experimental data indicate that spontaneous and irregular motor pattern genesis can derive from a cell-specific pacemaker mechanism involving an intracellular calcium dynamic that itself is strictly periodic, but where randomness arises from cycle-to-cycle variations in the amplitude of the rhythmic membrane depolarizations it produces. By oscillating close to the threshold for voltage-dependent plateau potential genesis required for CPG circuit output, these low-amplitude depolarizations thereby determine the variability with which *Aplysia's* exploratory movements are expressed. Timing irregularity would be further reinforced by an interaction between the differing dynamics of the organelle-derived and voltage-dependent oscillatory mechanisms that coexist in the B63 neuron as mentioned above.

Magnitude alterations in cytosolic calcium fluxes and resultant plasma membrane voltage changes can arise from an interaction between different dynamic processes. Such variability could result from a direct interplay between the different intracellular calcium stores themselves (Geiger and Magoski, 2008; Groten et al., 2013; Haberichter et al., 2001; Hajnóczky et al., 1995; Wacquier et al., 2019, 2016) or from an interaction between the store-generated calcium oscillation and extracellular calcium influxes (Chay, 1996a; Falcke et al., 2000; van Helden et al., 2000). Furthermore, voltage amplitude irregularity could arise from an interplay between the individual calcium oscillations of gap junction-coupled neurons (Bindschadler and Sneyd, 2001; De Blasio et al., 2004; Liu et al., 2011). In addition to such processes, irregular magnitude fluctuations in the voltage oscillation of the B63 neurons could also partly result from plateau potential production in the different electrically-coupled neurons of the buccal

CPG network. Presumably, because these plateaus are generated in the soma, far from the intercellular junctions in the neuropile, they are not phase-coupled in the different network neurons, producing only weak depolarizations in post-junctional cell partners. Nevertheless, these uncoordinated depolarizations would be sufficient to participate in randomly modifying the amplitude of the ongoing voltage oscillation in the B63 neurons.

Propagation of pacemaker activity amongst gap junction-connected neurons

It is well known that gap junction-mediated electrical coupling promotes the synchronization of pacemaker neuron bursting in CPG networks (Leznik and Llinás, 2005; Marder, 1984; Nadim et al., 2017; Sasaki et al., 2013; Sieling et al., 2014; Soto-Treviño et al., 2005), and is similarly involved in *Aplysia's* buccal feeding circuit (Sieling et al., 2014). In non-neuronal tissues, gap junctions have also been found to co-ordinate multicellular activity by propagating calcium waves via metabolic coupling (Benninger et al., 2008; Leybaert and Sanderson, 2012; Peters et al., 2007). Due to strong intracellular buffering mechanisms, calcium itself is unlikely to play a role in such intercellular communication (Leybaert and Sanderson, 2012). Rather, calcium wave propagation through gap junctions is most likely mediated by a diffusion of IP3 and its chain activation of IP3/Ry receptors and calcium release within adjacent cells (Harootunian et al., 1991; Miyazaki et al., 1992; Takeuchi et al., 2020). In addition to transfer through gap junctions, calcium waves can be propagated by extracellular paracrine signaling involving calcium-induced ATP release and an activation of ATP-gated membrane receptors and resultant IP3 synthesis in neighboring cells (Newman and Zahs, 1997; Scemes and Giaume, 2006).

552 Several lines of evidence suggest that the calcium dynamic driving membrane potential
553 oscillation and originating in the B63 neurons is also conveyed non-electrically to its gap
554 junction-coupled partners in the buccal network. First, the magnitude of B63's voltage
555 oscillation, which is presumably proportional to the intracellular calcium signal, was
556 consistently stronger than in any other network cells, such as B30, B31 and B65, despite their
557 similar membrane input resistances. Second, the voltage oscillation in B63 preceded that
558 recorded in these other cells by several seconds, which is compatible with a slower propagation
559 (~70 µm/s) of the underlying calcium oscillatory signal by a metabolic process rather than by
560 direct electrical transmission of the voltage oscillation itself (Benninger et al., 2008). Third, the
561 intracellular injection of the IP3 receptor antagonist heparin into B63, but not into B31,
562 suppressed the voltage oscillation in both neurons, thus indicating that its origin and
563 intercellular propagation is selectively dependent on IP3 signaling in B63. These findings also
564 argue against the possibility that the oscillation occurring throughout the buccal CPG circuit is a
565 network property that emerges from electrical coupling between equivalently-active neurons,
566 but rather, further underline the crucial pacemaker role played by B63 in buccal network
567 operation. In contrast to all other identified circuit cells, this neuron pair are the only elements
568 necessary and sufficient for triggering buccal motor pattern expression and resultant food-
569 seeking movement (Hurwitz et al., 1997; Nargeot et al., 2009). Moreover, this essential leading
570 role persists after appetitive operant conditioning-when the network's junctional conductances
571 are strengthened and the transition from irregular to rhythmic BMP genesis occurs (Nargeot et
572 al., 2009; Nargeot and Simmers, 2012).

573 In conclusion, without excluding the involvement of other cellular mechanisms, our
574 study shows that in the absence of extrinsic stimulation, the CPG network output for *Aplysia's*
575 food-seeking behavior can arise from a combination of spontaneous intracellular calcium
576 dynamics in two decision neurons and IP3-dependent circuit-wide metabolic propagation.
577 Although autonomously bursting neurons may employ intracellular stores as a source of
578 calcium (Kadiri et al., 2011; Levy, 1992; Scholz et al., 1988), in all cases, the mobilization of store
579 calcium, by interacting with calcium-activated membrane channels, is thought to regulate the
580 voltage dynamics of ongoing bursting behavior. However, other than theoretical evidence
581 (Chay, 1996a, 1996b), a spontaneous and rhythmic organelle-derived calcium dynamic serving
582 as a primary oscillator mechanism for actually driving neuronal bursting has not been previously
583 reported. Moreover, we believe that our findings provide the first example of the involvement
584 of such a rhythmogenic mechanism in the highly variable expression of a motivated behavior.
585 Experiments are now required to determine whether B63's intracellular calcium handling is
586 regulated by associative learning when hungry *Aplysia* switches its impulsive and irregular food-
587 seeking movements to a rhythmic compulsive-like act as found in more complex organisms.
588

Materials and Methods

Animals

Adult *Aplysia californica* (purchased from the University of Florida, Florida), and *A. fasciata* (caught locally in the Bassin d'Arcachon, France) were used in the experiments. Consistent with previous studies (Katzoff et al., 2002; Sieling et al., 2014), no inter-species differences in either behavioral or neuronal characteristics were found. Animals were housed in tanks containing fresh aerated sea water (~15°C) and were fed *ad libitum* with seaweed (*Ulva lactuca* obtained from the Station Biologique at Roscoff*, France*).

Isolated nervous preparation

Animals were anesthetized with 50 ml isotonic $MgCl_2$ solution (in mM: 360 $MgCl_2$, 10 HEPES adjusted to pH 7.5) injected into the hemocoel. The bilateral buccal ganglia and their peripheral nerves were dissected from the animal and pinned out in a Sylgard-lined Petri dish containing a standard artificial sea water solution (ASW, in mM: 450 NaCl, 10 KCl, 30 $MgCl_2$, 20 $MgSO_4$, 10 $CaCl_2$, 10 HEPES with the pH adjusted to 7.5). The ganglia were desheathed to expose the neuronal somata and the preparations were continuously superfused with ASW at 15°C.

In vitro electrophysiology

Spontaneous buccal motor output patterns were monitored by wire electrodes placed against appropriate motor nerves and insulated from the bath with petroleum jelly (Vaseline). The I2

(I2 n.), 2,1 (n. 2,1) and radular (R n.) nerves were used to monitor radular protraction, retraction and closure activity, respectively (Nargeot et al., 1997). The motor pattern-initiating interneurons B63 and B30, and the motoneurons B31/B32 (protraction) and B8 (closure) were recorded and identified according to previously reported criteria (Church and Lloyd, 1991; Hurwitz et al., 1997; Jelescu et al., 2013; Jing et al., 2004; Susswein and Byrne, 1988). These neurons were impaled with sharp glass microelectrodes with a tip resistance of 20-30 MΩ and filled with a KCH_3CO_2 solution (2 M). In the two-electrode current-clamp condition, two intrasomatic electrodes were inserted in each neuron, with one electrode used for current injection and the other for membrane potential recording via an Axoclamp-2B amplifier (Molecular Devices, Palo Alto, CA). Intracellular and extracellular signals were digitalized and acquired at 5 kHz with a CED interface (CED 1401, Cambridge Electronic Design, UK) with Spike 2 software (Cambridge Electronic Design, UK).

Modified saline and pharmacology

Blockade of chemical synaptic transmission was performed with bath perfusion of a modified ASW that contained cobalt, a calcium channel blocker ($CoCl_2$, 10 mM), and a lowered concentration of calcium ($CaCl_2$, 3 mM) (Alkon and Grossman, 1978). Neither this decrease in Ca^{2+} concentration alone, nor the presence of the $CoCl_2$ alone was found sufficient to block the chemical synapses. This 'Low Ca+Co' saline contained (in mM): 446 NaCl, 10 KCl, 30 $MgCl_2$, 20 $MgSO_4$, 3 $CaCl_2$, 10 $CoCl_2$, 10 HEPES with the NaCl concentration adjusted to the same osmolarity as ASW. Synaptic blockade was indicated by the suppression of chemical excitatory post-synaptic potentials produced by B63 in the contralateral B31 neuron (Hurwitz et al., 1997).

Data reported here under the Low Ca+Co saline condition were acquired after 20 min perfusion to allow for a complete synaptic blockade and the recovery of recorded neurons' resting membrane potential to at least -50 mV.

The sodium- or calcium-free solutions used in several experiments derived from modifications to the Low Ca+Co saline. In the Na^{+}-free saline, sodium was totally substituted by choline (in mM: 446 $C_5H_{14}NO.Cl$, 10 KCl, 30 $MgCl_2$, 20 $MgSO_4$, 3 $CaCl_2$, 10 $CoCl_2$, 10 HEPES). In the Ca^{2+}-free saline, no calcium was present and a calcium chelator, Ethylene glycol-bis (2-aminoethylether)-N, N, N ', N'-tetraacetic acid (EGTA) was added to the solution (in mM: 450 NaCl, 10 KCl, 30 $MgCl_2$, 20 $MgSO_4$, 10 $CoCl_2$, 10 HEPES, 0.5 EGTA) (Hickey et al., 2010). The pH for all solutions was adjusted to 7.5.

Tetrodotoxin (TTX, Tocris), a blocker of sodium channels in plasma membranes, was diluted to 50 µM in distilled water from a 0.5 mM stock solution (Hurwitz et al., 2008). Cyclopianozic acid (CPA, Merck-Sigma-Aldrich), a blocker of the sarco/endoplasmic reticulum Ca^{2+}-ATPase pump (SERCA) and Carbonyl cyanide 4- (trifluoromethoxy) phenylhydrazone (FCCP, Merck-Sigma-Aldrich), a protonophoric uncoupler of mitochondrial oxidative phosphorylation that depolarizes the mitochondrial membrane and leads to the organelle's release of calcium, were diluted to 20 µM in Low Ca+Co saline from stock solutions that were prepared in dimethyl sulfoxide (DMSO) (Benz and McLaughlin, 1983; Geiger and Magoski, 2008; Hickey et al., 2010). The maximum concentration of DMSO in the final volume reached 0.05%, which in control and previously reported studies did not alter the electrophysiological properties of neurons, the strength of electrical synapses, or intracellular calcium concentrations (Beekharry et al., 2018).

Heparin sodium salt solution (Tocris) at 20 mg/ml, an inositol tri-phosphate (IP3) receptor antagonist (Bezin et al., 2008), was pressure injected via an glass micropipette (10 MΩ) inserted into the cell bodies of the bilateral B63 or B31 neurons. Pressure was generated by a Picospritzer2 with 20 pulses of 15 PSI, 150 ms, at around 0.03 Hz. Following injection, which was performed during bath perfusion of ASW, one of the 2 heparin-containing electrodes was removed and replaced by a 2 M KAcetate microelectrode for intracellular recording that started 30 min after the heparin injection. In several of these experiments (2/5 with B63 and 2/4 with B31), 2 mg/ml of fast green (Merck-Sigma-Aldrich) was added to the heparin solution to verify effectiveness of the injection. No difference was found between the intracellular recordings of cells injected with or without fast green.

Intracellular recording analysis

Variations in the membrane potential of recorded neurons were analyzed in a cycle frequency/period bandwidth of 0.00195 to 0.125 Hz (i.e., periods of 512 s to 8 s) by Fast Fourier Transform (FFT) analysis using R language and environment (R Core Team, 2019) for statistical computing. The membrane voltage recordings were initially smoothed using the Spike 2 'Smooth' filter with a time constant of 500 ms to suppress signals of frequencies higher than those within the desired band-width and down-sampled at 1 Hz in order to decrease computation time. The resulting power spectral density periodograms were then used to identify oscillation periods of peak magnitude (Supplemental Figure 1). The periodograms were computed from the FFT frequency spectrograms by converting the frequency band (in Hz) to its reciprocal, period (in secs), to facilitate discerning the temporal correspondence between these

675 plots and the relatively slow (from secs to mins) spontaneous membrane voltage fluctuations
676 occurring in the raw recordings. Reconstruction of the sinusoidal waveforms corresponding to
677 dominant periods and the phase-relationships between signals from neuron pairs were
678 computed from Wavelet decomposition using the R-CRAN "WaveletComp" package for the
679 built-in analysis of univariate and bivariate time series (Roesch and Schmidbauer, 2018).
680 Averaged periodograms represent means +/- 95% confidence interval (CI95%) of the individual
681 periodograms. Phase-plane plots of membrane potential were computed by using custom-
682 written R script for intracellular recordings that were smoothed with a time constant of 500 ms
683 and down-sampled at 10 Hz.
684

685 **Statistical analyses**

686 Animals were randomly assigned to each experimental group, and although estimations of
687 sample sizes were not computed initially, an attempt was made to minimize the number of
688 animals sacrificed. One-sample comparisons to a theoretical value (0 sec.) were performed
689 using the two-tailed one-sample Wilcoxon signed rank test (V_0 statistic). Within-group
690 comparisons of two datasets were carried out using the two-tailed Wilcoxon signed rank test (V
691 statistic). Between-group comparisons for more than two independent groups were conducted
692 using the two-tailed Kruskal-Wallis test (H statistic) followed by the *post-hoc* multiple
693 comparisons Conover's test (q statistic). The application of these non-parametric statistical
694 tests to small datasets was justified by the failure to satisfy assumptions of normality and
695 homoscedasticity with high statistical powers. Statistical analyses were performed using the R-
696 CRAN "Base" and "PMCMRplus" packages (Pohlert, 2019). Similar results were obtained with

analyses performed both with and without outlier values, and all statistics reported in the text and figures were computed without data removal. Differences were considered significant for $p < 0.05$. Box-plot illustrations represent median values (horizontal lines) along with the first and third quartiles (boxes) in datasets.

Acknowledgements:

This research was supported by grants ANImE ANR-13-BV5-0014-01 (ANImE, R.N.), ANR-10-Idex-03-02 (A.B.), and a doctoral studentship (L.P.) from the French 'Ministère de l'Enseignement Supérieur et de la Recherche'.

Competing interests:

The authors declare that no competing interests exist.

References

Adams WB, Benson JA. 1985. The generation and modulation of endogenous rhythmicity in the aplysia bursting pacemaker neurone R15. *Progress in Biophysics and Molecular Biology* **46**:1–49. doi:10.1016/0079-6107(85)90011-2

Alkon DL, Grossman Y. 1978. Evidence for nonsynaptic neuronal interaction. *J Neurophysiol* **41**:640–653. doi:10.1152/jn.1978.41.3.640

Baker SA, Drumm BT, Saur D, Hennig GW, Ward SM, Sanders KM. 2016. Spontaneous Ca(2+) transients in interstitial cells of Cajal located within the deep muscular plexus of the murine small intestine. *J Physiol* **594**:3317–3338. doi:10.1113/JP271699

Bal T, Nagy F, Moulins M. 1988. The pyloric central pattern generator in Crustacea: a set of conditional neuronal oscillators. *Journal of Comparative Physiology A* **163**:715–727. doi:10.1007/BF00604049

Balleine BW. 2019. The Meaning of Behavior: Discriminating Reflex and Volition in the Brain. *Neuron* **104**:47–62. doi:10.1016/j.neuron.2019.09.024

Balleine BW, Dezfouli A. 2019. Hierarchical Action Control: Adaptive Collaboration Between Actions and Habits. *Front Psychol* **10**:2735. doi:10.3389/fpsyg.2019.02735

Beekharry CC, Gu Y, Magoski NS. 2018. Protein kinase C enhances electrical synaptic transmission by acting on junctional and postsynaptic Ca2+ Currents. *J Neurosci* **38**:2796–2808. doi:10.1523/JNEUROSCI.2619-17.2018

Benninger RKP, Zhang M, Head WS, Satin LS, Piston DW. 2008. Gap junction coupling and calcium waves in the pancreatic islet. *Biophys J* **95**:5048–5061. doi:10.1529/biophysj.108.140863

Benz R, McLaughlin S. 1983. The molecular mechanism of action of the proton ionophore FCCP (carbonylcyanide p-trifluoromethoxyphenylhydrazone). *Biophys J* **41**:381–398. doi:10.1016/S0006-3495(83)84449-X

Berridge KC. 2019. Affective valence in the brain: modules or modes? *Nat Rev Neurosci* **20**:225–234. doi:10.1038/s41583-019-0122-8

Berridge KC. 2004. Motivation concepts in behavioral neuroscience. *Physiol Behav* **81**:179–209. doi:10.1016/j.physbeh.2004.02.004

Bezin S, Charpentier G, Lee HC, Baux G, Fossier P, Cancela J-M. 2008. Regulation of nuclear Ca2+ signaling by translocation of the Ca2+ messenger synthesizing enzyme ADP-ribosyl cyclase during neuronal depolarization. *J Biol Chem* **283**:27859–27870. doi:10.1074/jbc.M804701200

Bindschadler M, Sneyd J. 2001. A bifurcation analysis of two coupled calcium oscillators. *Chaos* **11**:237–246. doi:10.1063/1.1342161

Brembs B, Lorenzetti FD, Reyes FD, Baxter DA, Byrne JH. 2002. Operant reward learning in Aplysia: neuronal correlates and mechanisms. *Science* **296**:1706–1709. doi:10.1126/science.1069434

Brocard F, Shevtsova NA, Bouhadfane M, Tazerart S, Heinemann U, Rybak IA, Vinay L. 2013. Activity-dependent changes in extracellular Ca2+ and K+ reveal pacemakers in the spinal locomotor-related network. *Neuron* **77**:1047–1054. doi:10.1016/j.neuron.2013.01.026

Butera RJ, Clark JW, Byrne JH. 1996. Dissection and reduction of a modeled bursting neuron. *J Comput Neurosci* **3**:199–223. doi:10.1007/BF00161132

Calabrese RL. 1995. Oscillation in motor pattern-generating networks. *Curr Opin Neurobiol* **5**:816–823. doi:10.1016/0959-4388(95)80111-1

Canavier CC, Clark JW, Byrne JH. 1991. Simulation of the bursting activity of neuron R15 in Aplysia: role of ionic currents, calcium balance, and modulatory transmitters. *J Neurophysiol* **66**:2107–2124. doi:10.1152/jn.1991.66.6.2107

Carroll MS, Ramirez J-M. 2013. Cycle-by-cycle assembly of respiratory network activity is dynamic and stochastic. *J Neurophysiol* **109**:296–305. doi:10.1152/jn.00830.2011

Chay TR. 1996a. Electrical bursting and luminal calcium oscillation in excitable cell models. *Biol Cybern* **75**:419–431. doi:10.1007/s004220050307

Chay TR. 1996b. Modeling slowly bursting neurons via calcium store and voltage-independent calcium current. *Neural Comput* **8**:951–978. doi:10.1162/neco.1996.8.5.951

Chevalier M, Toporikova N, Simmers J, Thoby-Brisson M. 2016. Development of pacemaker properties and rhythmogenic mechanisms in the mouse embryonic respiratory network. *Elife* **5**. doi:10.7554/eLife.16125

Church PJ, Lloyd PE. 1991. Expression of diverse neuropeptide cotransmitters by identified motor neurons in Aplysia. *J Neurosci* **11**:618–625.

Costa RM, Baxter DA, Byrne JH. 2020. Computational model of the distributed representation of operant reward memory: combinatoric engagement of intrinsic and synaptic plasticity mechanisms. *Learn Mem* **27**:236–249. doi:10.1101/lm.051367.120

772 Cullins MJ, Gill JP, McManus JM, Lu H, Shaw KM, Chiel HJ. 2015. Sensory Feedback Reduces
773 Individuality by Increasing Variability within Subjects. *Curr Biol* **25**:2672–2676.
774 doi:10.1016/j.cub.2015.08.044
775 Darbon P, Tscherter A, Yvon C, Streit J. 2003. Role of the electrogenic Na/K pump in
776 disinhibition-induced bursting in cultured spinal networks. *J Neurophysiol* **90**:3119–
777 3129. doi:10.1152/jn.00579.2003
778 Darshan R, Wood WE, Peters S, Leblois A, Hansel D. 2017. A canonical neural mechanism for
779 behavioral variability. *Nat Commun* **8**:15415. doi:10.1038/ncomms15415
780 De Blasio BF, Iversen J-G, Røttingen J-A. 2004. Intercellular calcium signalling in cultured
781 renal epithelia: a theoretical study of synchronization mode and pacemaker activity. *Eur*
782 *Biophys J* **33**:657–670. doi:10.1007/s00249-004-0409-0
783 Dickinson A, Balleine B. 1994. Motivational control of goal-directed action. *Animal Learning &*
784 *Behavior* **22**:1–18.
785 Everitt BJ, Robbins TW. 2016. Drug Addiction: Updating Actions to Habits to Compulsions Ten
786 Years On. *Annu Rev Psychol* **67**:23–50. doi:10.1146/annurev-psych-122414-033457
787 Everitt BJ, Robbins TW. 2005. Neural systems of reinforcement for drug addiction: from actions
788 to habits to compulsion. *Nat Neurosci* **8**:1481–1489. doi:10.1038/nn1579
789 Falcke M, Huerta R, Rabinovich MI, Abarbanel HD, Elson RC, Selverston AI. 2000. Modeling
790 observed chaotic oscillations in bursting neurons: the role of calcium dynamics and IP3.
791 *Biol Cybern* **82**:517–527. doi:10.1007/s004220050604
792 Fridlyand LE, Tamarina N, Philipson LH. 2010. Bursting and calcium oscillations in pancreatic
793 beta-cells: specific pacemakers for specific mechanisms. *Am J Physiol Endocrinol Metab*
794 **299**:E517-532. doi:10.1152/ajpendo.00177.2010
795 Fujimoto A, Hori Y, Nagai Y, Kikuchi E, Oyama K, Suhara T, Minamimoto T. 2019. Signaling
796 Incentive and Drive in the Primate Ventral Pallidum for Motivational Control of Goal-
797 Directed Action. *J Neurosci* **39**:1793–1804. doi:10.1523/JNEUROSCI.2399-18.2018
798 Geiger JE, Magoski NS. 2008. Ca2+-induced Ca2+ release in Aplysia bag cell neurons requires
799 interaction between mitochondrial and endoplasmic reticulum stores. *J Neurophysiol*
800 **100**:24–37. doi:10.1152/jn.90356.2008
801 Golowasch J, Bose A, Guan Y, Salloum D, Roeser A, Nadim F. 2017. A balance of outward and
802 linear inward ionic currents is required for generation of slow-wave oscillations. *J*
803 *Neurophysiol* **118**:1092–1104. doi:10.1152/jn.00240.2017
804 Grillner S, El Manira A. 2020. Current Principles of Motor Control, with Special Reference to
805 Vertebrate Locomotion. *Physiol Rev* **100**:271–320. doi:10.1152/physrev.00015.2019
806 Groten CJ, Rebane JT, Blohm G, Magoski NS. 2013. Separate Ca2+ sources are buffered by
807 distinct Ca2+ handling systems in aplysia neuroendocrine cells. *J Neurosci* **33**:6476–
808 6491. doi:10.1523/JNEUROSCI.6384-11.2013
809 Gu X, Olson EC, Spitzer NC. 1994. Spontaneous neuronal calcium spikes and waves during
810 early differentiation. *J Neurosci* **14**:6325–6335. doi:10.1523/JNEUROSCI.14-11-
811 06325.1994
812 Haberichter T, Marhl M, Heinrich R. 2001. Birhythmicity, trirhythmicity and chaos in bursting
813 calcium oscillations. *Biophys Chem* **90**:17–30. doi:10.1016/s0301-4622(01)00127-2
814 Hajnóczky G, Robb-Gaspers LD, Seitz MB, Thomas AP. 1995. Decoding of cytosolic calcium
815 oscillations in the mitochondria. *Cell* **82**:415–424. doi:10.1016/0092-8674(95)90430-1

816 Harootunian AT, Kao JP, Paranjape S, Tsien RY. 1991. Generation of calcium oscillations in
817 fibroblasts by positive feedback between calcium and IP3. *Science* **251**:75–78.
818 doi:10.1126/science.1986413
819 Harris-Warrick RM. 2002. Voltage-sensitive ion channels in rhythmic motor systems. *Curr Opin*
820 *Neurobiol* **12**:646–651. doi:10.1016/s0959-4388(02)00377-x
821 Harris-Warrick RM, Flamm RE. 1987. Multiple mechanisms of bursting in a conditional
822 bursting neuron. *J Neurosci* **7**:2113–2128.
823 Hickey CM, Geiger JE, Groten CJ, Magoski NS. 2010. Mitochondrial Ca2+ activates a cation
824 current in Aplysia bag cell neurons. *J Neurophysiol* **103**:1543–1556.
825 doi:10.1152/jn.01121.2009
826 Hurwitz I, Kupfermann I, Susswein AJ. 1997. Different roles of neurons B63 and B34 that are
827 active during the protraction phase of buccal motor programs in Aplysia californica. *J*
828 *Neurophysiol* **78**:1305–1319. doi:10.1152/jn.1997.78.3.1305
829 Hurwitz I, Ophir A, Korngreen A, Koester J, Susswein AJ. 2008. Currents contributing to
830 decision making in neurons B31/B32 of Aplysia. *J Neurophysiol* **99**:814–830.
831 doi:10.1152/jn.00972.2007
832 Jelescu IO, Nargeot R, Le Bihan D, Ciobanu L. 2013. Highlighting manganese dynamics in the
833 nervous system of Aplysia californica using MEMRI at ultra-high field. *Neuroimage*
834 **76**:264–271. doi:10.1016/j.neuroimage.2013.03.022
835 Jing J, Cropper EC, Hurwitz I, Weiss KR. 2004. The construction of movement with behavior-
836 specific and behavior-independent modules. *J Neurosci* **24**:6315–6325.
837 doi:10.1523/JNEUROSCI.0965-04.2004
838 Johnson SW, Seutin V, North RA. 1992. Burst firing in dopamine neurons induced by N-methyl-
839 D-aspartate: role of electrogenic sodium pump. *Science* **258**:665–667.
840 doi:10.1126/science.1329209
841 Kadiri LR, Kwan AC, Webb WW, Harris-Warrick RM. 2011. Dopamine-induced oscillations of
842 the pyloric pacemaker neuron rely on release of calcium from intracellular stores. *J*
843 *Neurophysiol* **106**:1288–1298. doi:10.1152/jn.00456.2011
844 Katzoff A, Ben-Gedalya T, Susswein AJ. 2002. Nitric oxide is necessary for multiple memory
845 processes after learning that a food is inedible in Aplysia. *J Neurosci* **22**:9581–9594.
846 Koshiya N, Smith JC. 1999. Neuronal pacemaker for breathing visualized in vitro. *Nature*
847 **400**:360–363. doi:10.1038/22540
848 Kramer RH, Zucker RS. 1985. Calcium-dependent inward current in Aplysia bursting pace-
849 maker neurones. *J Physiol* **362**:107–130. doi:10.1113/jphysiol.1985.sp015666
850 Kueh D, Barnett WH, Cymbalyuk GS, Calabrese RL. 2016. Na(+)/K(+) pump interacts with the
851 h-current to control bursting activity in central pattern generator neurons of leeches. *Elife*
852 **5**. doi:10.7554/eLife.19322
853 Kupfermann I. 1974. Feeding behavior in Aplysia: a simple system for the study of motivation.
854 *Behav Biol* **10**:1–26. doi:10.1016/s0091-6773(74)91644-7
855 Levy S. 1992. Effect of intracellular injection of inositol trisphosphate on cytosolic calcium and
856 membrane currents in Aplysia neurons. *J Neurosci* **12**:2120–2129.
857 doi:10.1523/JNEUROSCI.12-06-02120.1992
858 Leybaert L, Sanderson MJ. 2012. Intercellular Ca(2+) waves: mechanisms and function. *Physiol*
859 *Rev* **92**:1359–1392. doi:10.1152/physrev.00029.2011
860 Leznik E, Llinás R. 2005. Role of gap junctions in synchronized neuronal oscillations in the
861 inferior olive. *J Neurophysiol* **94**:2447–2456. doi:10.1152/jn.00353.2005

Liu P, Chen B, Wang Z-W. 2011. Gap junctions synchronize action potentials and Ca2+ transients in Caenorhabditis elegans body wall muscle. *J Biol Chem* **286**:44285–44293. doi:10.1074/jbc.M111.292078

Liu Z, Golowasch J, Marder E, Abbott LF. 1998. A model neuron with activity-dependent conductances regulated by multiple calcium sensors. *J Neurosci* **18**:2309–2320.

Lyttle DN, Gill JP, Shaw KM, Thomas PJ, Chiel HJ. 2017. Robustness, flexibility, and sensitivity in a multifunctional motor control model. *Biol Cybern* **111**:25–47. doi:10.1007/s00422-016-0704-8

Marder E. 1984. Roles for electrical coupling in neural circuits as revealed by selective neuronal deletions. *J Exp Biol* **112**:147–167.

Marder E, Goeritz ML, Otopalik AG. 2015. Robust circuit rhythms in small circuits arise from variable circuit components and mechanisms. *Curr Opin Neurobiol* **31**:156–163. doi:10.1016/j.conb.2014.10.012

Mathieu PA, Roberge FA. 1971. Characteristics of pacemaker oscillations in Aplysia neurons. *Can J Physiol Pharmacol* **49**:787–795. doi:10.1139/y71-108

McManus JM, Chiel HJ, Susswein AJ. 2019. Successful and unsuccessful attempts to swallow in a reduced Aplysia preparation regulate feeding responses and produce memory at different neural sites. *Learn Mem* **26**:151–165. doi:10.1101/lm.048983.118

Melanson A, Mejias JF, Jun JJ, Maler L, Longtin A. 2017. Nonstationary Stochastic Dynamics Underlie Spontaneous Transitions between Active and Inactive Behavioral States. *eNeuro* **4**. doi:10.1523/ENEURO.0355-16.2017

Miller JP, Selverston AI. 1982. Mechanisms underlying pattern generation in lobster stomatogastric ganglion as determined by selective inactivation of identified neurons. II. Oscillatory properties of pyloric neurons. *J Neurophysiol* **48**:1378–1391. doi:10.1152/jn.1982.48.6.1378

Miyazaki S, Yuzaki M, Nakada K, Shirakawa H, Nakanishi S, Nakade S, Mikoshiba K. 1992. Block of Ca2+ wave and Ca2+ oscillation by antibody to the inositol 1,4,5-trisphosphate receptor in fertilized hamster eggs. *Science* **257**:251–255. doi:10.1126/science.1321497

Nadim F, Li X, Gray M, Golowasch J. 2017. Chapter 4 - The Role of Electrical Coupling in Rhythm Generation in Small Networks In: Jing J, editor. Network Functions and Plasticity. Academic Press. pp. 51–78. doi:10.1016/B978-0-12-803471-2.00004-7

Nargeot R, Baxter DA, Byrne JH. 1997. Contingent-dependent enhancement of rhythmic motor patterns: an in vitro analog of operant conditioning. *J Neurosci* **17**:8093–8105.

Nargeot R, Le Bon-Jego M, Simmers J. 2009. Cellular and network mechanisms of operant learning-induced compulsive behavior in Aplysia. *Curr Biol* **19**:975–984. doi:10.1016/j.cub.2009.05.030

Nargeot R, Petrissans C, Simmers J. 2007. Behavioral and in vitro correlates of compulsive-like food seeking induced by operant conditioning in Aplysia. *J Neurosci* **27**:8059–8070. doi:10.1523/JNEUROSCI.1950-07.2007

Nargeot R, Simmers J. 2012. Functional organization and adaptability of a decision-making network in aplysia. *Front Neurosci* **6**:113. doi:10.3389/fnins.2012.00113

Newman EA, Zahs KR. 1997. Calcium waves in retinal glial cells. *Science* **275**:844–847. doi:10.1126/science.275.5301.844

Pearson KG. 2000. Neural adaptation in the generation of rhythmic behavior. *Annu Rev Physiol* **62**:723–753. doi:10.1146/annurev.physiol.62.1.723

907 Peña F, Parkis MA, Tryba AK, Ramirez J-M. 2004. Differential Contribution of Pacemaker
908 Properties to the Generation of Respiratory Rhythms during Normoxia and Hypoxia.
909 *Neuron* **43**:105–117. doi:10.1016/j.neuron.2004.06.023
910 Peters MA, Teramoto T, White JQ, Iwasaki K, Jorgensen EM. 2007. A calcium wave mediated
911 by gap junctions coordinates a rhythmic behavior in C. elegans. *Curr Biol* **17**:1601–1608.
912 doi:10.1016/j.cub.2007.08.031
913 Pohlert T. 2019. PMCMRplus: Calculate Pairwise Multiple Comparisons of Mean Rank Sums
914 Extended.
915 R Core Team. 2019. R: a language and environment for statistical computing. Vienne, Austria.
916 Roesch A, Schmidbauer H. 2018. WaveletComp: Computational Wavelet Analysis.
917 Sasaki K, Cropper EC, Weiss KR, Jing J. 2013. Functional differentiation of a population of
918 electrically coupled heterogeneous elements in a microcircuit. *J Neurosci* **33**:93–105.
919 doi:10.1523/JNEUROSCI.3841-12.2013
920 Scemes E, Giaume C. 2006. Astrocyte calcium waves: what they are and what they do. *Glia*
921 **54**:716–725. doi:10.1002/glia.20374
922 Scholz KP, Cleary LJ, Byrne JH. 1988. Inositol 1,4,5-trisphosphate alters bursting pacemaker
923 activity in Aplysia neurons: voltage-clamp analysis of effects on calcium currents.
924 *Journal of Neurophysiology* **60**:86–104. doi:10.1152/jn.1988.60.1.86
925 Selverston AI. 2010. Invertebrate central pattern generator circuits. *Philos Trans R Soc Lond B*
926 *Biol Sci* **365**:2329–2345. doi:10.1098/rstb.2009.0270
927 Sieling F, Bédécarrats A, Simmers J, Prinz AA, Nargeot R. 2014. Differential roles of
928 nonsynaptic and synaptic plasticity in operant reward learning-induced compulsive
929 behavior. *Curr Biol* **24**:941–950. doi:10.1016/j.cub.2014.03.004
930 Sims DW, Humphries NE, Hu N, Medan V, Berni J. 2019. Optimal searching behaviour
931 generated intrinsically by the central pattern generator for locomotion. *Elife* **8**.
932 doi:10.7554/eLife.50316
933 Soto-Treviño C, Rabbah P, Marder E, Nadim F. 2005. Computational model of electrically
934 coupled, intrinsically distinct pacemaker neurons. *J Neurophysiol* **94**:590–604.
935 doi:10.1152/jn.00013.2005
936 Steuer I, Guertin PA. 2019. Central pattern generators in the brainstem and spinal cord: an
937 overview of basic principles, similarities and differences. *Rev Neurosci* **30**:107–164.
938 doi:10.1515/revneuro-2017-0102
939 Susswein AJ, Byrne JH. 1988. Identification and characterization of neurons initiating patterned
940 neural activity in the buccal ganglia of Aplysia. *J Neurosci* **8**:2049–2061.
941 Susswein AJ, Hurwitz I, Thorne R, Byrne JH, Baxter DA. 2002. Mechanisms underlying fictive
942 feeding in aplysia: coupling between a large neuron with plateau potentials activity and a
943 spiking neuron. *J Neurophysiol* **87**:2307–2323. doi:10.1152/jn.2002.87.5.2307
944 Takeuchi Y, Narumi R, Akiyama R, Vitiello E, Shirai T, Tanimura N, Kuromiya K, Ishikawa S,
945 Kajita M, Tada M, Haraoka Y, Akieda Y, Ishitani T, Fujioka Y, Ohba Y, Yamada S,
946 Hosokawa Y, Toyama Y, Matsui T, Fujita Y. 2020. Calcium Wave Promotes Cell
947 Extrusion. *Current Biology* **30**:670-681.e6. doi:10.1016/j.cub.2019.11.089
948 Tam S, Hurwitz I, Chiel HJ, Susswein AJ. 2020. Multiple Local Synaptic Modifications at
949 Specific Sensorimotor Connections after Learning Are Associated with Behavioral
950 Adaptations That Are Components of a Global Response Change. *J Neurosci* **40**:4363–
951 4371. doi:10.1523/JNEUROSCI.2647-19.2020

van Helden DF, Imtiaz MS, Nurgaliyeva K, von der Weid P, Dosen PJ. 2000. Role of calcium stores and membrane voltage in the generation of slow wave action potentials in guinea-pig gastric pylorus. *J Physiol* **524 Pt 1**:245–265. doi:10.1111/j.1469-7793.2000.00245.x

Vinogradova TM, Maltsev VA, Bogdanov KY, Lyashkov AE, Lakatta EG. 2005. Rhythmic Ca2+ oscillations drive sinoatrial nodal cell pacemaker function to make the heart tick. *Ann N Y Acad Sci* **1047**:138–156. doi:10.1196/annals.1341.013

Wacquier B, Combettes L, Van Nhieu GT, Dupont G. 2016. Interplay Between Intracellular Ca 2+ Oscillations and Ca 2+ -stimulated Mitochondrial Metabolism. *Scientific Reports* **6**:19316. doi:10.1038/srep19316

Wacquier B, Voorsluijs V, Combettes L, Dupont G. 2019. Coding and decoding of oscillatory Ca2+ signals. *Seminars in Cell & Developmental Biology*, SI: Calcium signalling **94**:11–19. doi:10.1016/j.semcdb.2019.01.008

Wimmer K, Compte A, Roxin A, Peixoto D, Renart A, de la Rocha J. 2015. Sensory integration dynamics in a hierarchical network explains choice probabilities in cortical area MT. *Nat Commun* **6**:6177. doi:10.1038/ncomms7177

Yu X, Byrne JH, Baxter DA. 2004. Modeling interactions between electrical activity and second-messenger cascades in Aplysia neuron R15. *J Neurophysiol* **91**:2297–2311. doi:10.1152/jn.00787.2003

Zhang G, Yu K, Wang T, Chen T-T, Yuan W-D, Yang F, Le Z-W, Guo S-Q, Xue Y-Y, Chen S-A, Yang Z, Liu F, Cropper EC, Weiss KR, Jing J. 2020. Synaptic mechanisms for motor variability in a feedforward network. *Sci Adv* **6**. doi:10.1126/sciadv.aba4856

Zhou Y, Lv M, Li T, Zhang T, Duncan R, Wang L, Lu XL. 2019. Spontaneous calcium signaling of cartilage cells: from spatiotemporal features to biophysical modeling. *FASEB J* **33**:4675–4687. doi:10.1096/fj.201801460R

Zhu L, Selverston AI, Ayers J. 2016. Role of Ih in differentiating the dynamics of the gastric and pyloric neurons in the stomatogastric ganglion of the lobster, Homarus americanus. *J Neurophysiol* **115**:2434–2445. doi:10.1152/jn.00737.2015

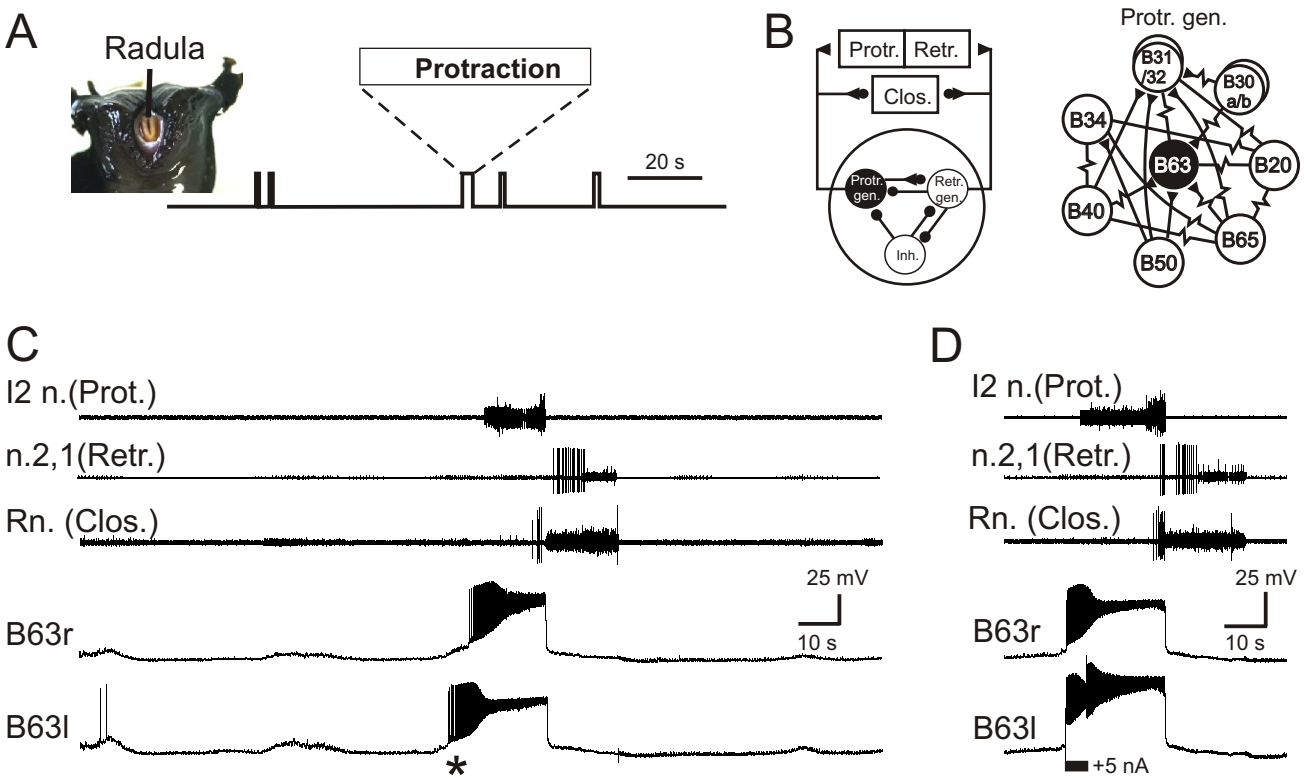

Figure 1. Aplysia's spontaneous radula biting behavior and underlying motor pattern generation.

(A) In vivo food-seeking behavior. In the absence of any external stimulation, Aplysia's radula (see head frontal view at left) spontaneously produces biting movements consisting of irregularly-timed cycles of radula protraction (upward deflection of movement monitor trace), closure and retraction (downward deflection).

(B) Schematics of the buccal CPG network that generates radula biting movements. Left: simplified diagram of the half-center network (one in each of the bilateral buccal ganglia) and its synaptic connections with protraction (Protr.), retraction (Retr.) and closure (Clos.) motoneurons (filled circles and triangles; inhibitory and excitatory connections, respectively). The network producing each bi-phasic cycle of movement is composed of three distinct and synaptically connected neuronal subsets comprising a protraction generator (Protr. gen.), a retraction generator (Retr. gen.) and a group of inhibitory neurons (Inh.). Right: detailed schematic of identified neurons belonging to the protraction generator and their synaptic interconnections (filled triangles, excitatory chemical synapses; resistance symbols, electrical synapses). Within the protraction generator, the neuron B63 (black) is necessary and sufficient to trigger the buccal motor pattern (BMP) for a radula bite cycle.

(C) Simultaneous extracellular recordings of a single BMP (top three traces) and intracellular recordings of the two bilateral and electrically-coupled B63 neurons (r, right; l, left) in an isolated in vitro buccal ganglia preparation. I2n., n.2,1, Rn., are respectively the motor nerves carrying axons of protractor, retractor and closure motor neurons. The two B63 cells expressed spontaneous and coincident membrane depolarizations (*) that initiated plateau potentials and associated impulse bursts, which in turn evoked a BMP by the buccal CPG network.

(D) Synchronous plateau potentials in the electrically-coupled B63 and a resulting BMP triggered by a brief intracellular depolarizing current pulse (+5 nA) injected into one (left) B63 neuron.

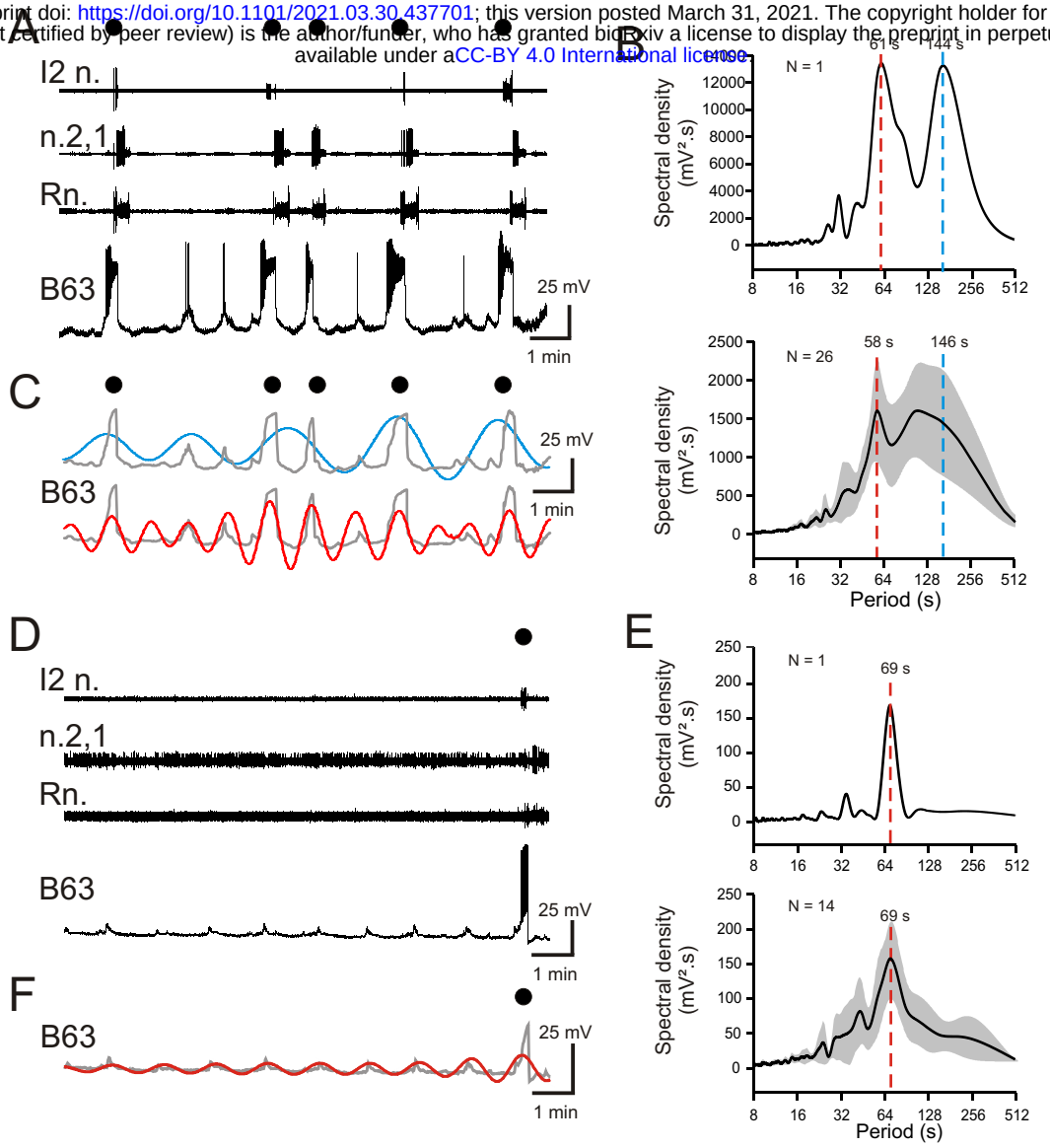

Figure 2. Periodicities in B63's spontaneous bioelectrical behavior.

(A) A 10 min recording excerpt of radula BMP genesis (black dots) in an in vitro buccal ganglion preparation showing associated spontaneous fluctuations in membrane potential of an intracellularly-recorded B63 neuron. Note that a BMP occurred only when B63 expressed prolonged burst firing driven by a plateau potential.

(B) Spectral density plot of the B63 recording illustrated in A (top) and the average power spectrum (± CI95%) from recordings of 26 different neurons (bottom). In both cases, the essentially bimodal periodograms indicated that the variations in B63's membrane potential comprised two distinct periodicities (indicated by red and blue dashed lines), which across all 26 neurons was 58 s and 146 s, respectively. For details see Supplemental Figure 1A.

(C) Wavelet-based reconstructions retaining the two dominant periods revealed in the individual power spectrum in B (top) and their superposition with the smoothed membrane voltage traces (gray) of the corresponding B63 neuron in A. The slower sinusoid (blue trace; period, 144 s) corresponded to the cell's strongest depolarizations associated exclusively with the expression of plateau potentials and resultant BMP genesis (black dots). The faster sinusoid (red trace; period, 61 s) corresponded to these supra-threshold depolarizations plus almost all remaining subthreshold depolarizations.

(D-F) Equivalent analyses of the same neurons as in A-C, but during recorded excerpts when no plateauing and BMP genesis occurred (N =14). The single plateau potential and BMP occurring at the end of the excerpt in D is illustrated for comparison with the B63 recording in A, but was not included in the spectral analyses of E (see Supplemental Figure 1B). In the absence of plateau potentials, the cells expressed spontaneous variations in membrane potential (D) composed of a single dominant, low-amplitude oscillation (E, F). Note that smaller additional peaks in the power spectra in B, E are essentially harmonics of the major period(s).

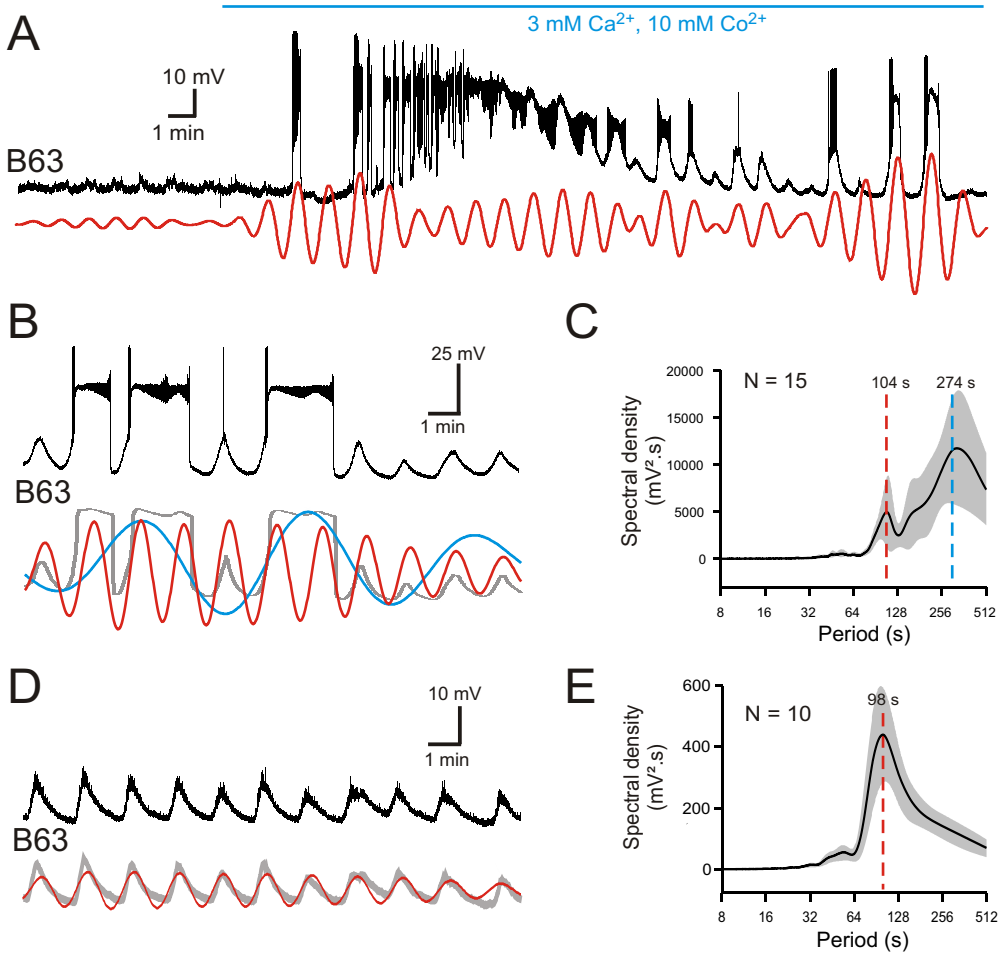

Figure 3. B63's voltage oscillations in the absence of functional chemical synapses.

(A) Membrane potential fluctuations and plateauing in a recorded B63 neuron immediately before and during onset of bath-applied Low Ca+Co saline (horizontal blue line) to block chemical synapses in the buccal CPG network. Red trace: corresponding reconstructed waveform from the peak spectral density (period range: 70-90 s).

(B,C) A different B63 cell recorded 20 min after onset of Low Ca+Co perfusion (B, Top trace; also see Supplemental Figure 1C). The membrane potential variations decomposed into two oscillatory waveforms (B, red and blue traces) with periods of 83 and 280 s, respectively. Gray trace: raw recording after smoothing. (C) Average power spectrum (mean period ± CI95%) from 15 neurons showing two major oscillations.

(D,E) Same analysis as in B,C, but of B63 recording sequences without plateau potential generation (also see Supplemental Figure 1D). The remaining spontaneous variations in membrane potential now comprised a single oscillation (D, red trace: period 85 s), as also indicated by the solitary dominant period in the averaged periodogram (mean ± CI95%) from 10 B63 neurons (E).

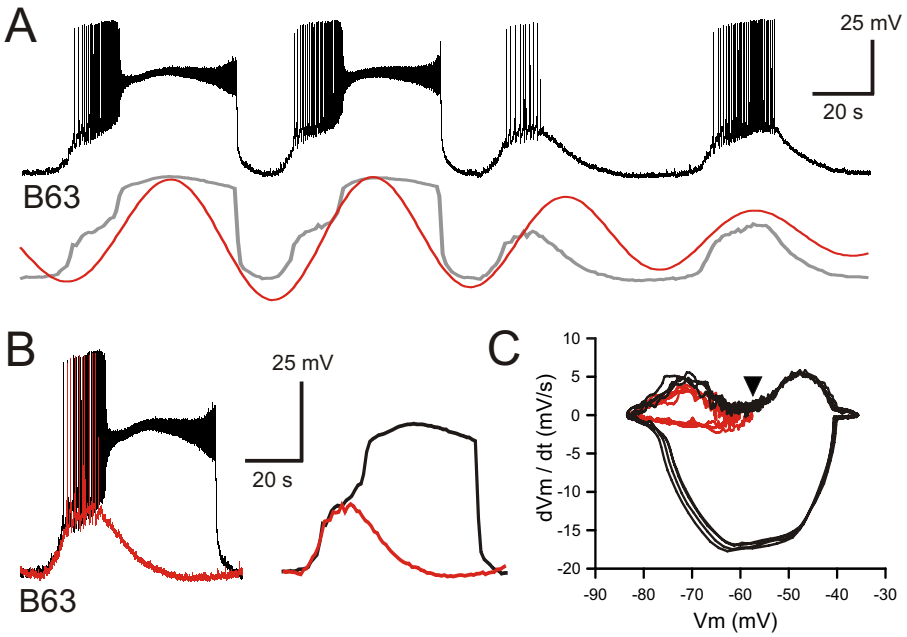

Figure 4. B63's voltage oscillation triggers plateau potentials.

(A) Intracellular recording of a B63 neuron under chemical synapse blockade during an excerpt in which each spontaneous voltage oscillation was associated (first two cycles) or not (last two cycles) with the expression of plateau potentials. Bottom traces: corresponding smoothed recording (gray trace) and reconstructed oscillation from the peak spectral density (red trace; period 64 s).

(B) Left: superposition of the first oscillation cycle in A with an accompanying plateau (black trace) and the third cycle without a plateau (red trace). Right: same traces after low-pass filtering to remove action potentials.

(C) Phase-plane plot of 8 successive oscillation cycles both without (4 cycles, red), and with (4 cycles, black) plateau potential generation in the same B63 neuron as in B, C. The initial raising phases of the sub- and supra-threshold depolarizations follow identical trajectories before either a return to baseline potential or a further depolarization into a prolonged plateau. The arrowhead indicates the voltage threshold for plateau potential generation.

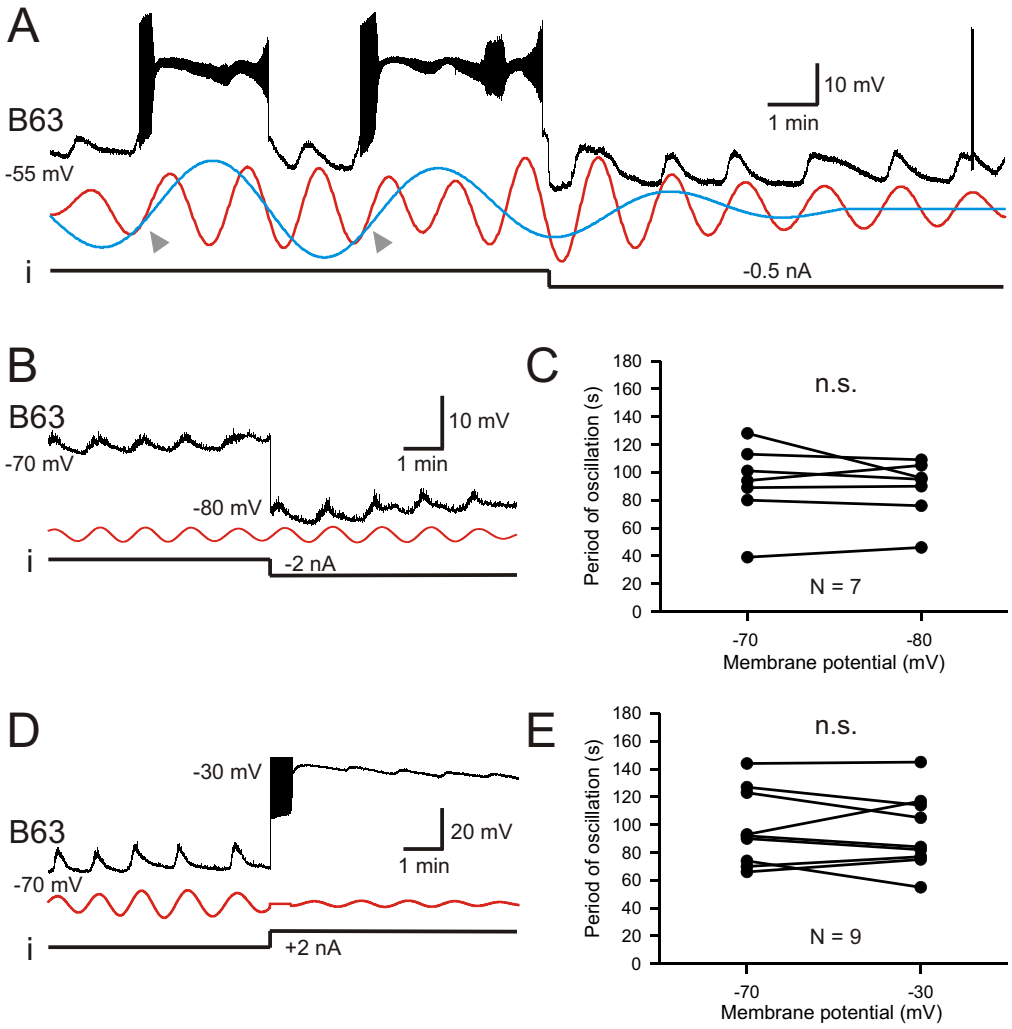

Figure 5. B63's low-amplitude oscillation does not arise from a voltage-sensitive mechanism.

(A) Under chemical synapse blockade (with Low Ca+Co saline), a B63 neuron's spontaneous plateau potentials, but not its low-amplitude voltage oscillation, is suppressed by continuous hyperpolarizing current injection (i, -0.5 nA). Red and blue traces: superimposed reconstructed waveforms from the peak spectral densities corresponding to the presence or absence of plateau potentials. Arrowheads indicate the points of waveform intersection where plateau potentials were initiated.

(B) Low-amplitude oscillation (upper trace) in a different B63 neuron during continuous hyperpolarization with chemical synapses blocked. The cell's membrane potential was held at -70 mV then stepped to -80 mV by continuous intracellular current injection (i) with two-electrode current clamp. Red trace: reconstructed waveform from the peak spectral density (period 80 s).

(C) The oscillation cycle periods of all 7 recorded neurons were not significantly (n.s.) modified by the same membrane potential manipulation ($V = 16$, $p = 0.799$).

(D,E) Same analysis as in B,C, but with the membrane potential initially held at -70, then depolarized to -30 mV with two-electrode current clamp (D). Red trace: reconstructed waveform from the peak spectral density (period: 70 s). (E) No significant difference (n.s.) in oscillation period in 9 recorded neurons at these two holding potentials ($V = 28$, $p = 0.553$).

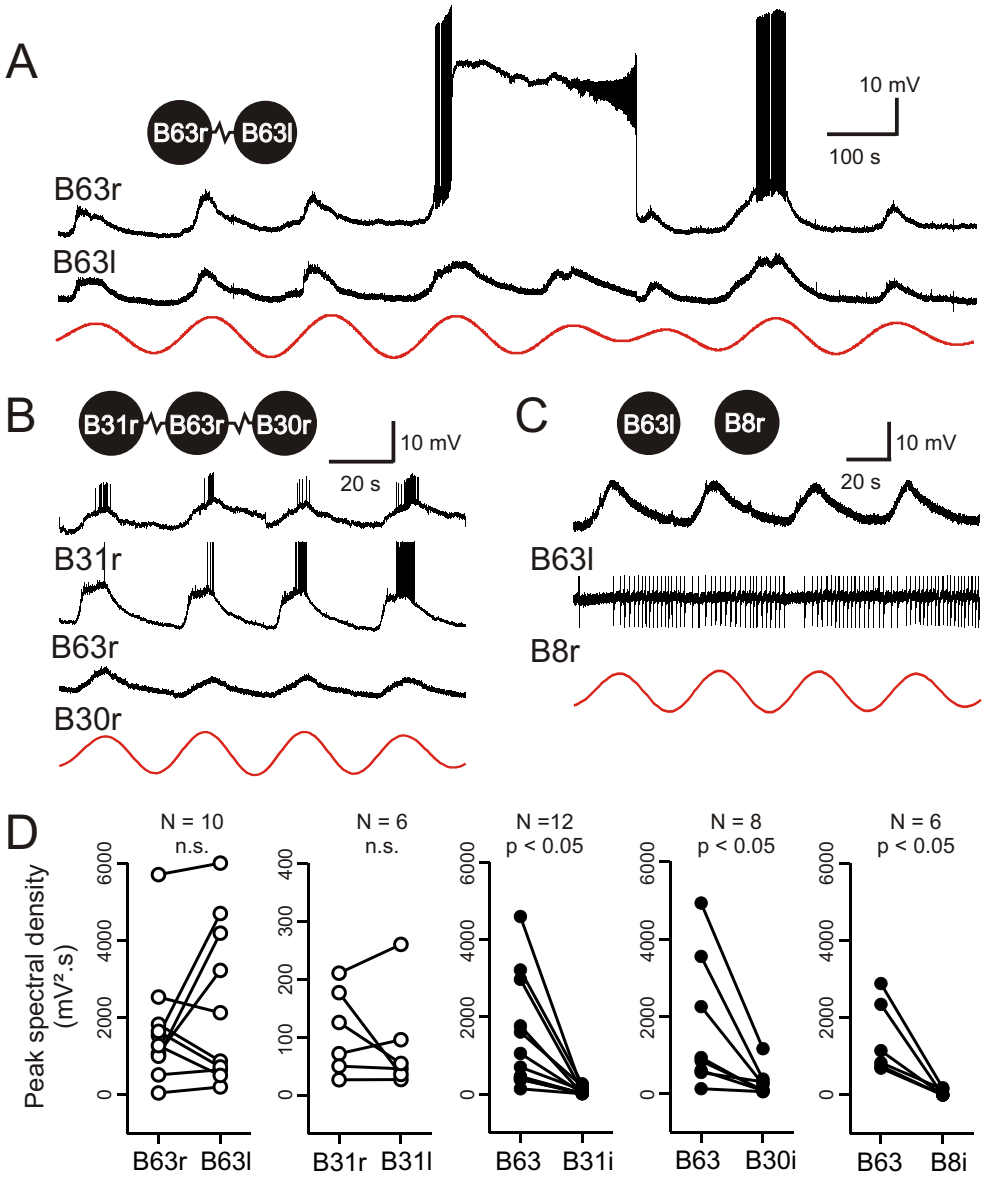

Figure 6. Low-amplitude oscillation in electrically-coupled network neurons.

(A,B) Simultaneous intracellular recordings from different protraction generator neurons under chemical synapse blockade. (A) Spontaneous membrane potential oscillations in the right (r) and left (l) electrically-coupled B63 cells (resistance symbol: electrical synapse). Note the independent expression of a plateau potential and burst firing in B63r. (B) Coordinated oscillations in a right B63 and ipsilateral, electrically-coupled B31 and B30 neurons (the action potentials in the B63 trace are truncated). Red traces in A and B: reconstructed waveforms from the peak spectral densities for B63l and B63r, respectively.

(C) Recordings from a B63 along with a non-coupled contralateral B8 motor neuron (action potentials in the B8 trace are truncated). A membrane voltage oscillation was absent in B8. Red trace: reconstructed waveform from the peak spectral density for B63.

(D) Comparison of oscillation magnitude (i.e., peak spectral amplitude) in contralateral (unfilled dots; l, left; r, right) and ipsilateral neurons (i, filled dots). The oscillation amplitude was not significantly different (n.s.) in bilateral homologous cells (white dots; B63r/B63l, V = 22, p = 0.625; B31r/B31l, V = 13, p = 0.688), but was significantly higher in B63 compared to heterologous neurons in the same (i, ipsilateral) ganglion (black dots; B63/B31i, V = 78, p = 0.005; B63/B30i, V = 36, p = 0.008; B63/B8i, V = 21, p = 0.031).

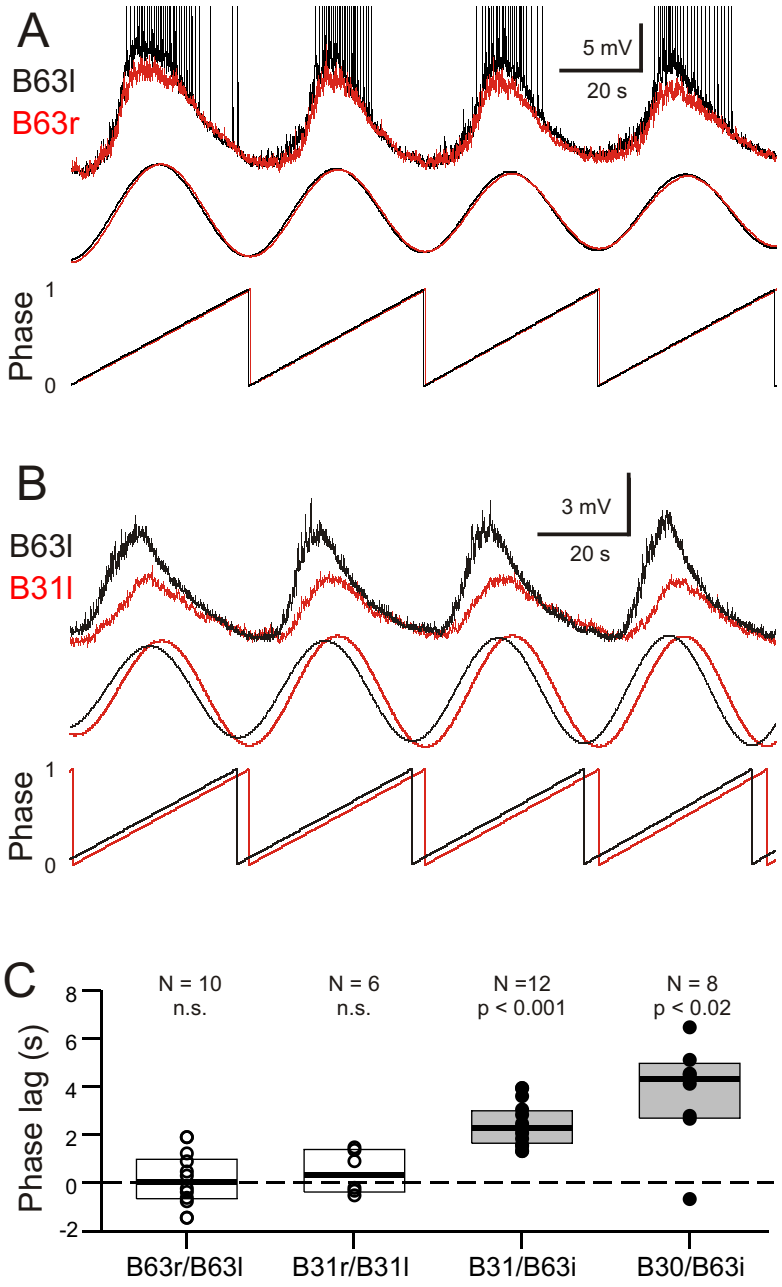

Figure 7. Phase-relationships between the oscillations of different network neurons.

(A,B) Upper traces: Superimposed phase-aligned intracellular recordings from different neuronal pairs - A), left (black) and right B63(red) ; B), left B63 (black) and left B31 (red) - under chemical synapse blockade (action potentials in B63l are truncated). Middle traces, reconstructed waveforms from the corresponding spectral periodograms after equivalence amplitude scaling. Lower traces: superimposed representations of the oscillation phases in each cell pair. No phase difference was evident between the two B63 neurons (A). In contrast, the oscillation of B63 (black) was phase-advanced relative to that of B31 (B).

(C) One-sample analyses showing that the oscillation phases in homologous bilateral neurons were not significantly (n.s.) different from zero (unfilled dots and boxes; B63r/B63l, V0 = 31, p = 0.770; B31r/B31l, V0 = 15, p = 0.438). In contrast, oscillations in heterologous neurons were significantly delayed (i.e., positive phase lag) relative to the ipsilateral (i) B63 partner (filled dots and boxes; B31/B63i, V0 = 78, p = 0.0005; B30/B63i, V0 = 35, p = 0.016).

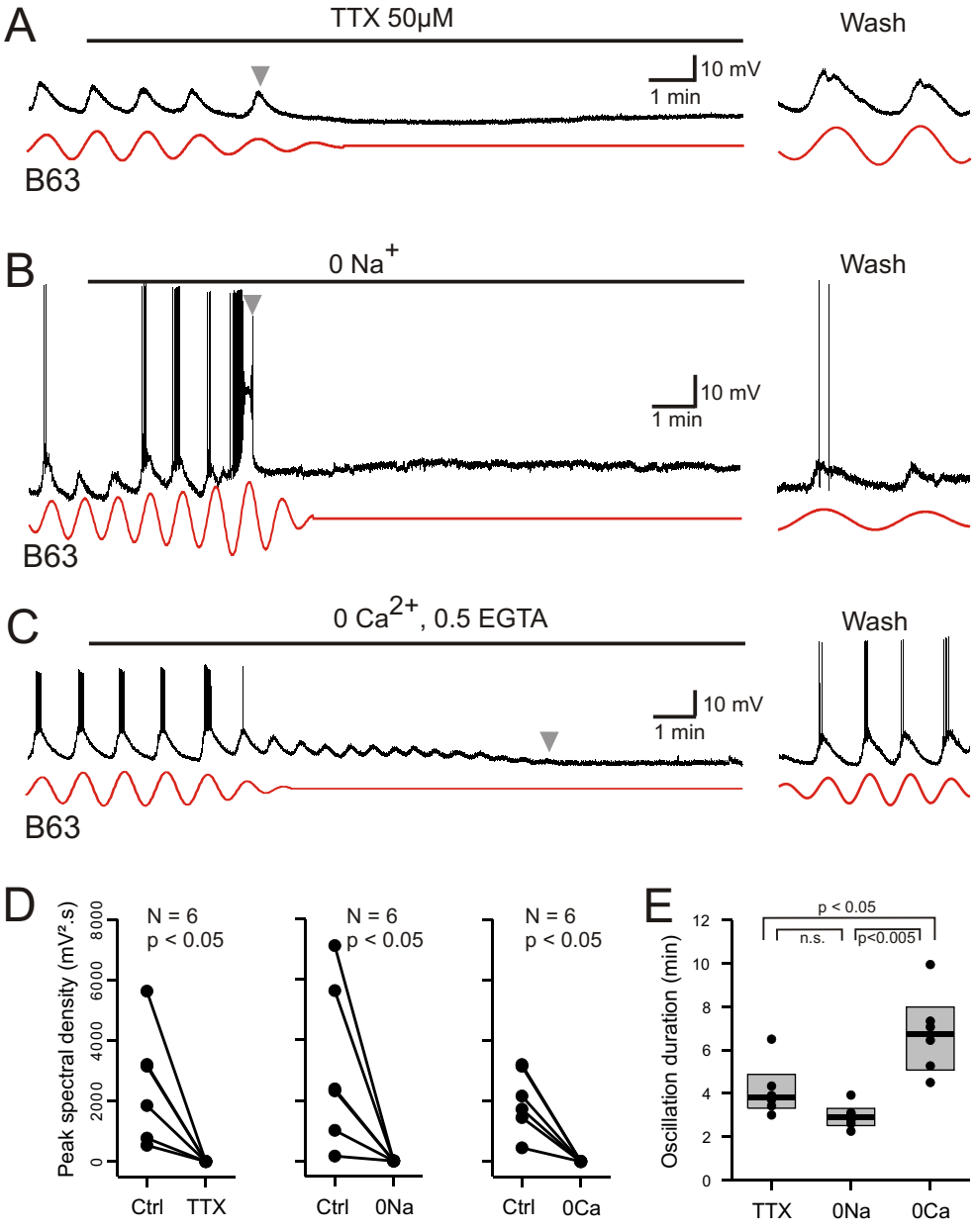

Figure 8. Involvement of sodium and calcium ions in the voltage oscillation.

(A-C) Under chemical synapse blockade, the spontaneous voltage oscillations of B63 neurons were reversibly (trace excerpts at right) suppressed by bath application of 50 µM tetrodotoxin (A, horizontal line), sodium-free (B, horizontal line) or calcium-free salines (C, horizontal line). Red traces: reconstructed waveforms from corresponding peak spectral densities.

(D) Group quantification under the experimental conditions illustrated in A-C: The amplitude of the dominant oscillation in Low Ca+Co saline alone (Control, Ctrl) was significantly reduced after application of TTX-containing (left, $V = -21$, $p = 0.031$), Na-free (middle, $V = -21$, $p = 0.031$), or calcium-free saline (right, $V = -21$, $p = 0.031$).

(E) Inter-group comparison of oscillation longevity (grey arrowheads in A-C) after modified-saline perfusion onset ($H = 11.684$, $p < 0.005$). B63's oscillation persisted for significantly longer after removal of extracellular calcium (0 Ca + 0.5 EGTA, $N = 6$) than after blockade of sodium channels by TTX ($N = 6$, $q = 4.625$, $p = 0.013$) or in the absence of extracellular Na ($N = 6$, $q = 8.092$, $p < 0.005$). No significant difference was evident between the effects of sodium channel blockade or Na removal ($q = -3.468$).

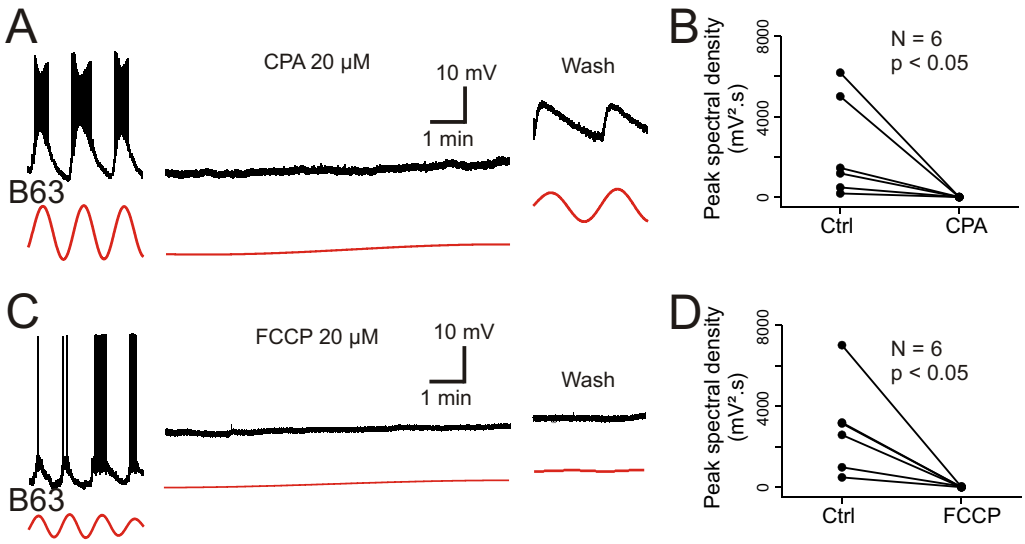

Figure 9. Involvement of intracellular calcium stores in the voltage oscillation.

(A) The spontaneous voltage oscillation of a B63 neuron (left excerpt) was reversibly (right excerpt) suppressed in the presence of 20 µM CPA, a SERC inhibitor (middle excerpt, recorded 20 min after the beginning of drug application).

(B) Group analysis showing a significant reduction in oscillation magnitude of 6 B63 neurons measured before (Ctrl) and 20 min after the beginning of CPA application ($V = 21$, $p = 0.031$).

(C) Suppression of B63 oscillation by application of 20 µM FCCP, an uncoupler of mitochondrial oxidative phosphorylation leading to calcium release. The neuron's spontaneous oscillation (left) was irreversibly (right) suppressed and the cell depolarized (middle, recorded 20 min after the beginning of drug application).

(D) The oscillation magnitudes (Ctrl) of 6 tested B63 neurons were significantly reduced ($V = 21$, $p = 0.031$) after 20 min of FCCP application.

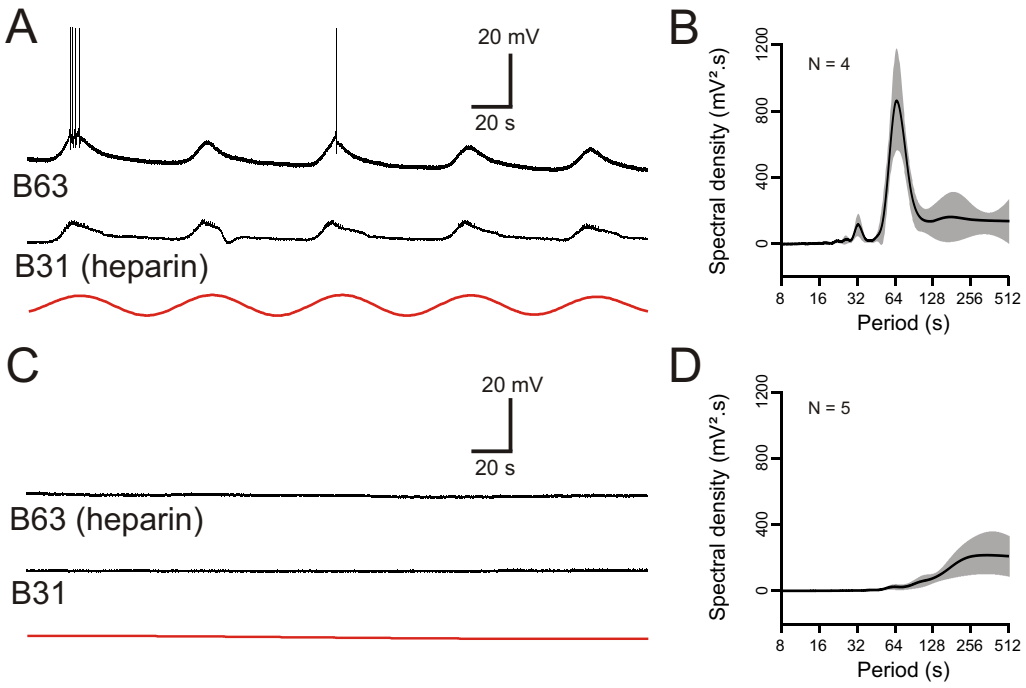

Figure 10. The voltage oscillation generated by intracellular calcium store release is specific to B63.

(A,C) Paired recordings of B63 and B31 neurons under chemical synapse blockade, 30 min after the beginning of an intrasomatic injection of the ER membrane calcium channel blocker heparin (20 mg/ml) into either the bilateral B31 (A) or bilateral B63 (C) neurons. Heparin in B31 had no effect on the ongoing oscillation of an un-injected B63 cell (A), but suppressed oscillations in both a B63 and an un-injected B31 (C) after injection into both B63 neurons. Red traces: reconstructed waveforms from the corresponding periodograms.

(B,D) Average power spectra obtained 30 min after the beginning of bilateral intracellular heparin injection into the B31 (B) or B63 neurons (D) in 4 and 5 preparations, respectively.

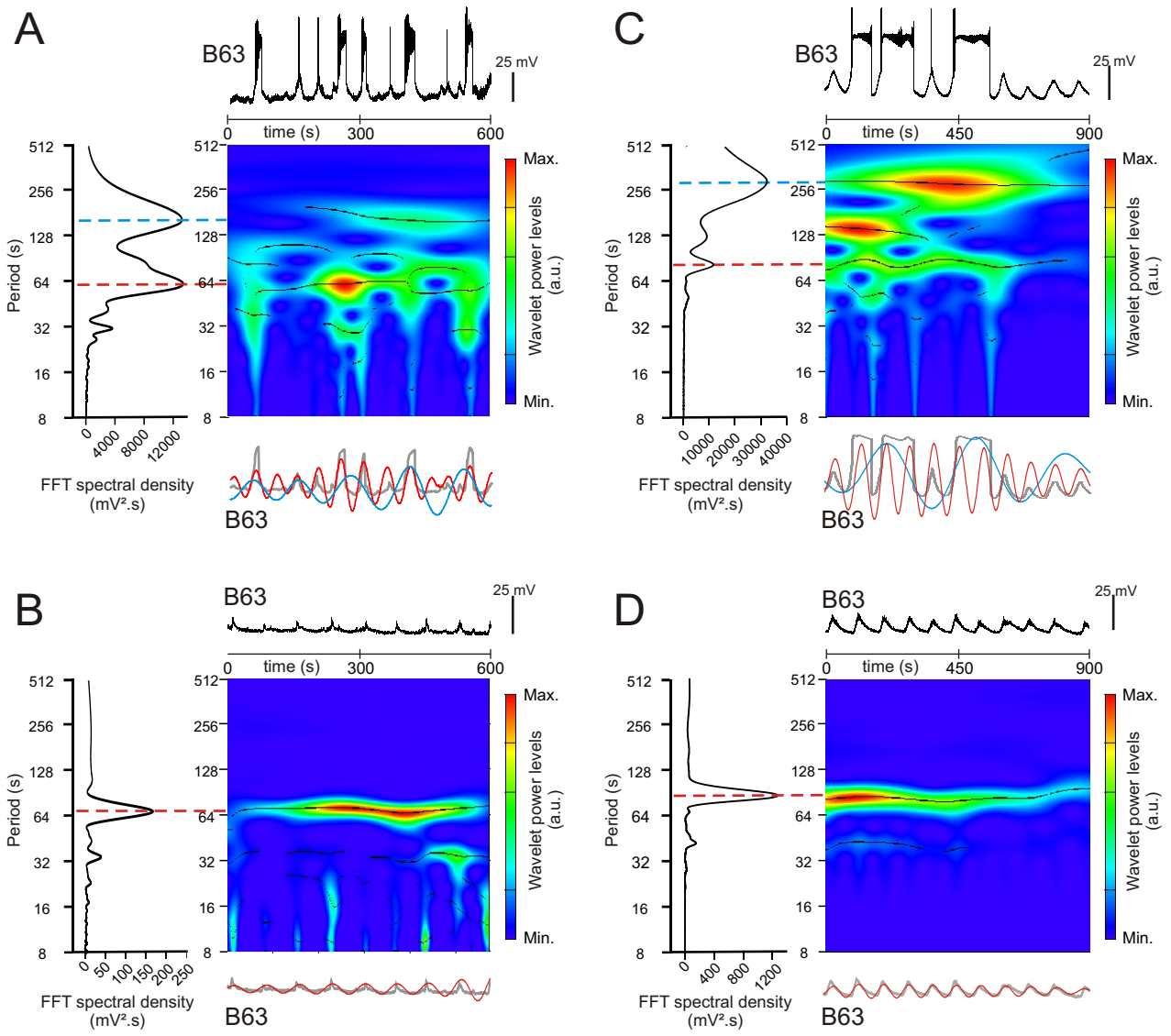

Supplemental Figure 1. Spectral density analysis of B63 neuron intracellular recordings.

A,B. Analysis under normal saline (ASW) conditions. Colored panels (middle) are wavelet-based power spectral decompositions of the membrane potential variations over time in the B63 cell recording excerpt shown at top (Color code bars: power; black lines: ridges of power). Plots at left are periodograms from Fast Fourrier Transform (FFT) of the same intracellular recordings used to quantify spectral densities (i.e., amplitudes) at dominant periods (indicated by red and blue lines) of voltage changes in the period range between 8 and 512 s. Note that event period (in secs) rather than its reciprocal (frequency) was used in the time domain due to the very slow spontaneous rates of membrane potential fluctuations (see Materials and Methods). Bottom traces are mathematically-reconstructed oscillations from the dominant periods revealed in the FFT periodograms (red and blue traces) superimposed with the corresponding intracellular recording excerpt after low pass filter smoothing to remove action potentials (gray traces). The recordings in A and B, and corresponding wavelet power spectra, periodograms and reconstructed oscillations, are from the same B63 neuron with (A) or without (B) the spontaneous expression of plateau potentials, as reported in Figure 2.

C,D. Equivalent analysis under Low Ca+Co saline conditions to block chemical synapses. The intracellular recordings (Top traces) and corresponding wavelet and FFT power spectral decomposition and reconstructed waveforms are from the same B63 neuron with (C) or without (D) spontaneous plateau potential generation, as reported in Figure 3.

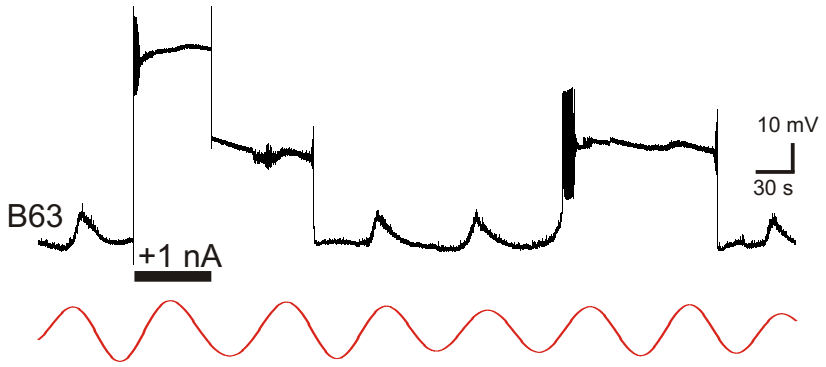

Supplemental Figure 2. B63 plateau potentials expressed with chemical synapses blocked.

Intracellular recording of a B63 neuron in a buccal ganglion under bath-applied Low Ca+Co saline. A transient intracellular injection of depolarizing current (horizontal bar, +1nA) elicited a prolonged plateau potential that was similar to a subsequent plateau triggered spontaneously on a depolarizing phase of ongoing membrane potential oscillation. The red trace is the corresponding reconstructed waveform from the peak spectral density; period 71 s.

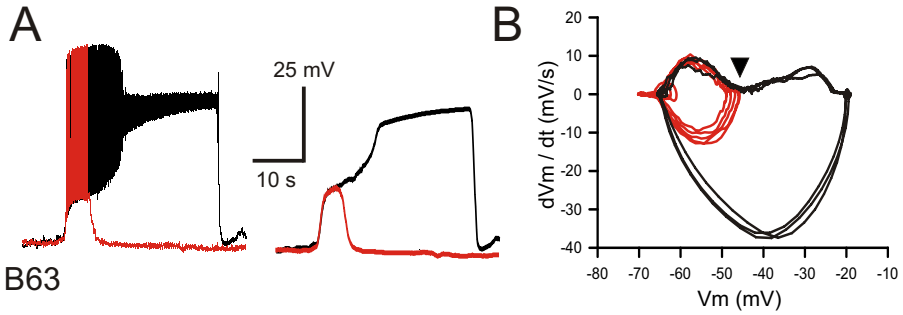

Supplemental Figure 3. B63's voltage oscillation triggers plateau potentials under normal saline (ASW) conditions.

A. Left: superposition of an oscillation cycle without a plateau (red trace) and one leading to a plateau (black trace) recorded in the absence of chemical synapse blockade. Right: same traces after low-pass filtering to remove action potentials.

B. Phase-plane plot of 8 successive oscillation cycles both without (5 cycles; red), and with (3 cycles; black) plateau potential generation in the same B63 neuron. The arrowhead indicates the voltage threshold for plateau potential generation.

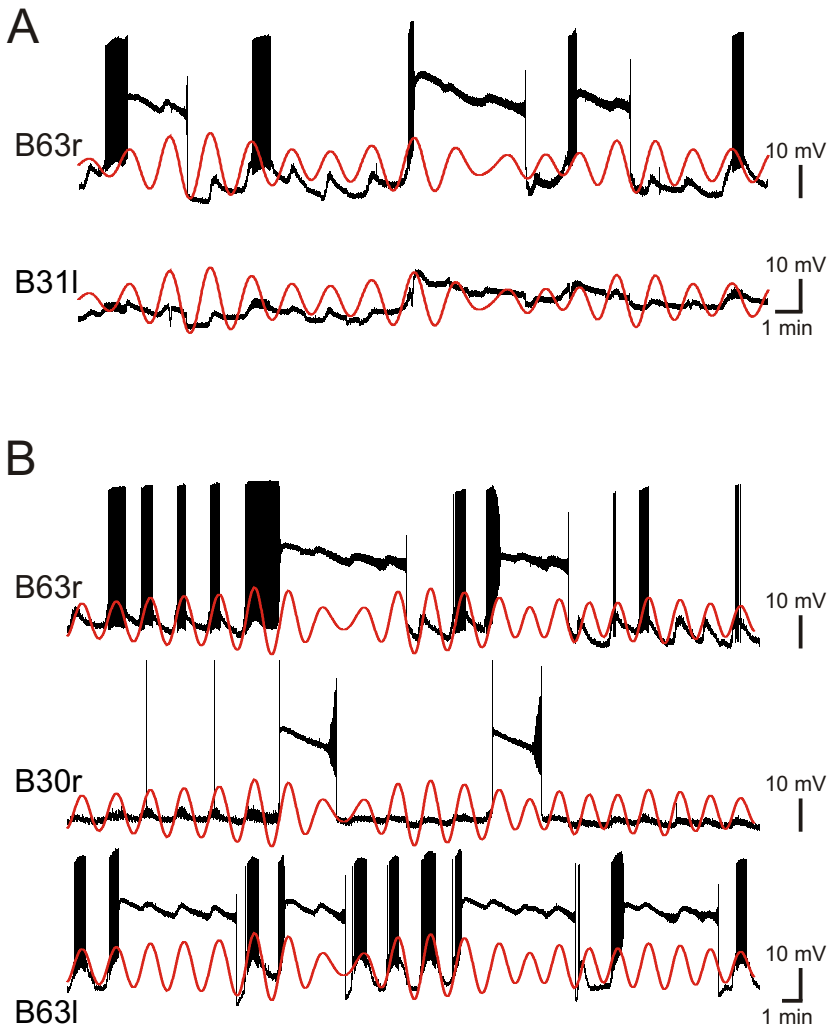

Supplemental Figure 4. Irregular plateau potentials triggered by regular voltage oscillations in electrically-coupled network neurons.

A. Paired intracellular recordings from two gap junction-coupled neurons (right B63 and left B31) under chemical synapse blockade. In contrast to the continuous synchronous and rhythmic depolarizations (see red traces, which are the reconstructed voltage oscillation of B63 superimposed with both the raw B63 and B31 recordings), the production of plateau potentials was irregular and occurred independently in the two neurons.

B. Simultaneous recordings from three gap junction-coupled neurons (right B63, right B30 and left B63) under chemical synapse blockade. All three cells expressed synchronous, rhythmic depolarizations (red traces: reconstructed voltage oscillation of right B63 superimposed with all raw recordings), but again, the onsets and terminations of plateau potentials were highly irregular within and between the individual neurons.

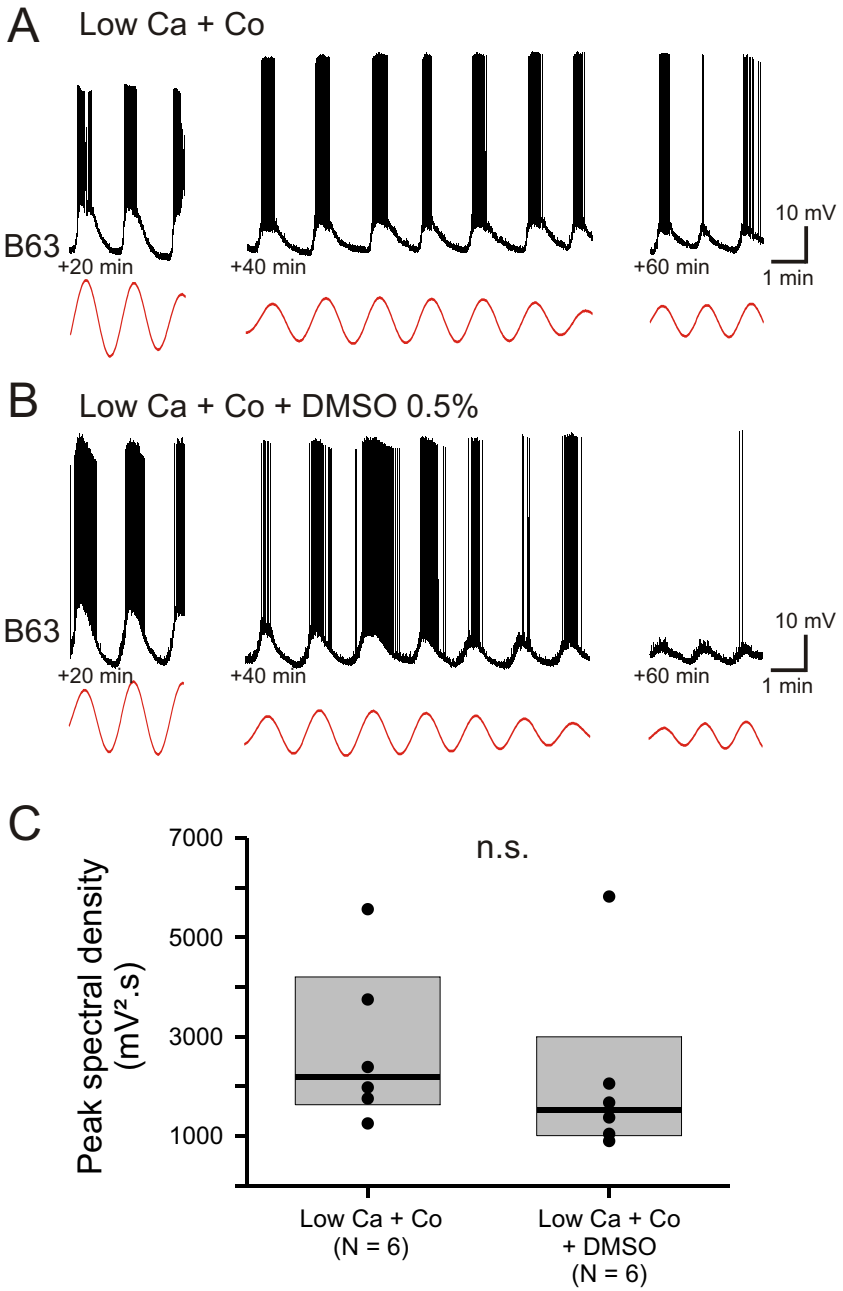

Supplemental Figure 5. The voltage oscillation of B63 is unaffected by exposure to DMSO.

A,B. Recordings from two different B63 neurons during bath-application of Low Ca+Co saline alone (A) or additionally containing 0.5% DMSO (B). Left trace excerpts: 20 min after the beginning of the perfusion. Middle traces: 40 min after perfusion onset. Right traces: 60 min after perfusion onset. Red traces: reconstructed waveforms from the corresponding peak spectral densities.

C. Group comparison of oscillation magnitudes in B63 cells measured from 20 until 30 min after the beginning of saline perfusion in the absence (left) and presence of 0.5% DMSO (right). DMSO had no significant (n.s.) effect on the amplitudes of the voltage oscillations (Mann-Whitney rank sum test: $V = 25$, $p = 0.310$).